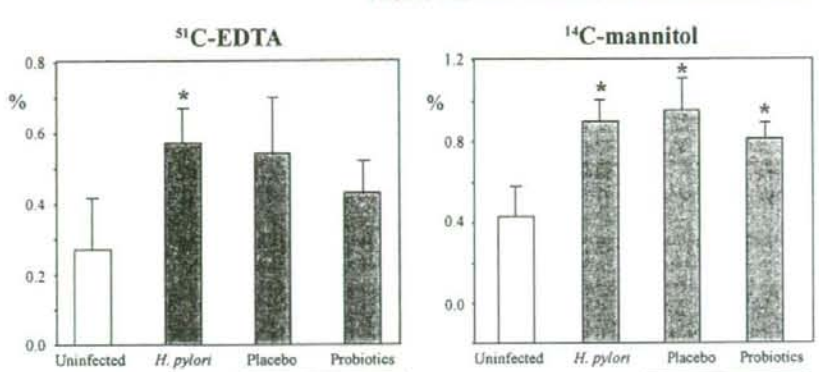


Fig. 5. Intestinal permeability for both $^{51}$C-EDTA and $^{14}$C-mannitol was increased in *H. pylori*-infected mice ($n$ = 16) compared with uninfected controls ($n$ = 7). Intestinal permeability tended to improve 2 mo posteradication in probiotic-treated mice ($n$ = 8) but did not reach statistical significance vs. placebo-treated mice ($n$ = 8). *$P$ < 0.05 vs. uninfected controls.

heightened immune response after luminal *H. pylori* antigen administration. In contrast, probiotic therapy significantly decreased the number of $CD3^+$ cells in the stomach of previously infected mice compared with placebo-treated mice in parallel with a faster recovery of gastric emptying. Thus the effect of probiotics on gastric emptying recovery may be mediated through a faster recovery of the chronic inflammatory response to *H. pylori*.

*H. pylori*-infected mice ate more frequently but smaller amounts of food per feeding bout compared with uninfected controls. This resulted in a similar total amount of food consumed per 24 h. The pattern is reminiscent of that observed frequently in patients with functional dyspepsia who have difficulty consuming regular size meals and therefore snack frequently throughout the day. Administration of probiotics normalized postinfective altered feeding behavior. It is possible that chronic inflammation in the stomach alters ascending neural pathways, resulting in abnormal feeding behavior, and that probiotics improve this through an effect on *H. pylori*-associated gastritis. However, other mechanisms such as direct modulation of neuroendocrine pathways by probiotics cannot be ruled out.

It has been shown that *H. pylori* infection alters gastric permeability in vivo and also on epithelial cell lines (6, 14, 15). The underlying mechanisms may include impaired mucus-bicarbonate barrier, disruption of tight junctions (occludin, ZO), and increase in transcellular permeability by *H. pylori*. These alterations may be long lasting and linked to chronic inflammation because bacterial eradication has been shown to improve gastric permeability only in those mice with significant improvement of chronic gastritis (14). A recent clinical study has suggested that intestinal permeability is altered in subjects with *H. pylori* infection (5). This may be more clinically relevant than changes in gastric permeability because the intestine represents a larger area of antigen and nutrient processing. The *H. pylori*-induced defect in intestinal barrier could result in chronic immune stimulation and bystander antigen stimulation even after *H. pylori* eradication. We measured permeability in ex vivo jejunal segments using a combination of two macromolecules to assess paracellular and membrane permeability. $^{51}$Cr-EDTA is an established marker for paracellular permeability, and $C^{14}$-mannitol is considered to be a marker for membrane permeability in in vivo studies. Both permeability to $^{51}$Cr-EDTA and mannitol were increased in *H. pylori*-infected mice. Bacterial eradication did not normalize intestinal permeability. Treatment with probiotics tended to improve paracellular permeability, but this did not achieve statistical significance compared with those previously infected and treated with placebo. Probiotics did not modify membrane permeability. In contrast to the probiotic-induced normalization of feeding behavior, combined administration of *L. rhamnosus* R0011 and *L. helveticus* R0052 had a modest effect on increased intestinal permeability after bacterial eradication. Thus resolution of altered feeding behavior and gastric emptying abnormalities by probiotics do not seem to be mediated principally by an improvement in small intestinal permeability in the chronic model of *H. pylori* infection. This finding is in disagreement with an earlier study using a stress model in the rat that showed that this combination of probiotic bacteria could protect against bacterial translocation (24). However, it supports the findings in an acute model of *H. pylori* in which *L. rhamnosus* R0011 and *L. helveticus* R0052 reduced *H. pylori*-induced antrum inflammation but not apoptosis (10).

In conclusion, using a murine model of chronic *H. pylori* infection and postinfective gut dysfunction we have shown that administration of *L. rhamnosus* R0011 and *L. helveticus* R0052 after *H. pylori* eradication accelerates recovery of gastric motor function and normalizes altered feeding behavior. This is associated with improvement in chronic gastric inflammation by probiotics but not with full recovery of intestinal barrier abnormalities. Treatment with luminal antigen related to the triggering infectious agent maintains gastric dysfunction long after bacterial eradication. The results suggest that specific probiotics may be useful in improving the rate of symptomatic relief in patients with dyspepsia after *H. pylori* eradication.

## GRANTS

This work was supported by a grant by the Canadian Institutes of Health Research (CIHR) (awarded to S. Collins) and by a grant by Institut Rosell-Lallemand (S. Collins). E. Verdu is supported by Canadian Association of Gastroenterology (CAG)/CIHR/Altana New Investigator Grant, Crohns and Colitis Foundation of Canada (CCFC) Innovation Grant, and holds a McMaster University Department of Medicine Internal Career Research Award. P. Bercik holds a McMaster University Department of Medicine Internal Career Research Award. This work was supported in part by Health and Labour Sciences Research Grants Ministry of Health, Labour and Welfare, Japan (H. Sakai and E. Tsuchida).

## REFERENCES


1. **Bercík P, Armstrong D, Emde C, Dutoit P, Fraser R, Blum AL, Kucera P.** Origin of rhythmic motility patterns in arterially perfused rat intestine. *Gastroenterology* 106: 649–657, 1994.
2. **Bercík P, De Giorgio R, Blennerhassett P, Verdú EF, Barbara G, Collins SM.** Immune-mediated neural dysfunction in a murine model of chronic *Helicobacter pylori* infection. *Gastroenterology* 123: 1205–1215, 2002.
3. **Bercik P, Wang L, Kean I, Verdu EF, Tougas G, Collins SM.** Persistence of sensory and eating disturbances after *H. pylori* eradication in mice. *Gastroenterology* 122: W1074, 2002. (Abstract)
4. **Blum AL, Talley NJ, O'Morrain C, van Zanten SV, Labenz J, Stolte M, Louw JA, Stubberod A, Theodors A, Sundin M, Bolling-Sternevald E, Junghard O.** Lack of effect of treating *Helicobacter pylori* infection in patients with non-ulcer dyspepsia. Omeprazole plus clarithromycin and amoxicillin effect one year after treatment (OCAY) study group. *N Engl J Med* 339: 1875–1881, 1998.
5. **Di Leo V, D'Inca R, Bettini MB, Podswiadek M, Punzi L, Mastropaolo G, Sturniolo GC.** Effect of *Helicobacter pylori* and eradication therapy on gastrointestinal permeability. Implications for patients with seronegative spondyloarthritis. *J Rheumatol* 32: 295–300, 2005.
6. **Fedwick JP, Lapointe TK, Meddings JB, Sherman PM, Buret AG.** *Helicobacter pylori* activates myosin light-chain kinase to disrupt claudin-4 and claudin-5 and increase epithelial permeability. *Infect Immun* 73: 7844–52, 2005.
7. **Graham DY, Klein PD.** Campylobacter pyloridis gastritis: the past, the present and speculations about the future (Review). *Am J Gastroenterol* 82: 283–286, 1987.
8. **Gwee KA, Graham JC, McKendrick MW, Collins SM, Marshall JS, Walters SJ, Read NW.** Psychometric scores and persistence of irritable bowel after infectious diarrhoea. *Lancet* 347: 150–153, 1996.
9. **Jiang B, Jordana M, Xing Z, Smaill F, Snider DP, Borojevic R, Steele-Norwood D, Hunt RH, Croitoru K.** Replication-defective adenovirus infection reduces *Helicobacter felis* colonization in the mouse in a gamma interferon- and interleukin-12-dependent manner. *Infect Immun* 67: 4539–4544, 1999.
10. **Johnson-Henry KC, Mitchell DJ, Avitzur Y, Galindo-Mata E, Jones NL, Sherman PM.** Probiotics reduce bacterial colonization and gastric inflammation in *H. pylori*-infected mice. *Dig Dis Sci* 49: 1095–1102, 2004.
11. **Malfertheiner P, Fischbach W, Layer P, Moessner J, Stolte M, Leodolter A, Demleitner K, Fuchs WA.** ELAN study proves symptomatic benefit of *Helicobacter pylori* eradication in functional dyspepsia. *Gastroenterology* 118: A440, 2000. (Abstract)
12. **Marshall JK, Thabane M, Garg AX, Clark WF, Salvadori M, Collins SM, Walkerton Health Study Investigators.** Incidence and epidemiology of irritable bowel syndrome after a large waterborne outbreak of bacterial dysentery. *Gastroenterology* 131: 445–450, 2006.
13. **Marshall BJ, Warren JR.** Unidentified curved bacilli in the stomach of patients with gastritis and peptic ulceration. *Lancet* 16: 1311–1315, 1984.
14. **Matysiak-Budnik T, Hashimoto K, Heyman M, de Mascarel A, Desjeux JF, Mégraud F.** Antral gastric permeability to antigens in mice is altered by infection with Helicobacter felis. *Eur J Gastroenterol Hepatol* 11: 1371–1377, 1999.
15. **Matysiak-Budnik T, Terpend K, Alain S, Sanson le Pors MJ, Desjeux JF, Mégraud F, Heyman M.** *Helicobacter pylori* alters exogenous antigen absorption and processing in a digestive tract epithelial cell line model. *Infect Immun* 66: 5785–5791, 1998.
16. **McColl K, Murray L, El-Omar E, Dickson A, El-Nujumi A, Wirz A, Kelman A, Penny C, Knill-Jones R, Hilditch T.** Symptomatic benefit from eradicating *Helicobacter pylori* infection in patients with non-ulcer dyspepsia. *N Engl J Med* 339: 1869–1874, 1998.
17. **Mearin F, Pérez-Oliveras M, Perelló A, Vinyet J, Ibañez A, Coderch J, Perona M.** Dyspepsia and irritable bowel syndrome after a *Salmonella* gastroenteritis outbreak: one-year follow-up cohort study. *Gastroenterology* 129: 98–104, 2005.
17a. **Sakai H, Sou K, Horinouchi H, Kobayashi K, Tsuchida E.** Hemoglobin vesicles as artificial oxygen carriers: present situation and future visions. *J Intern Med* 263: 4–15, 2008.
18. **Spiller RC, Jenkins D, Thornley JP, Hebden JM, Wright T, Skinner M, Neal KR.** Increased rectal mucosal enteroendocrine cells, T lymphocytes, and increased gut permeability following acute *Campylobacter* enteritis and in post-dysenteric irritable bowel syndrome. *Gut* 47: 804–811, 2000.
19. **Tack J, Demedts I, Dehondt G, Caenepeel P, Fischler B, Zandecki M, Janssens J.** Clinical and pathophysiological characteristics of acute-onset functional dyspepsia. *Gastroenterology* 122: 1738–1747, 2002.
20. **Talley NJ, Janssens J, Lauritsen K, Racz I, Bolling-Sternevald E.** Eradication of *Helicobacter pylori* in functional dyspepsia: randomised double blind placebo controlled trial with 12 mo' follow up. The optimal regimen cures *Helicobacter* induced dyspepsia (ORCHID) study group. *BMJ* 318: 833–837, 1999.
21. **Talley NJ, Vakil N, Ballard ED 2nd, Fenerty MB.** Absence of benefit of eradicating *Helicobacter pylori* in patients with non-ulcer dyspepsia. *N Engl J Med* 341: 1106–1111, 1999.
22. **Varghese AK, Verdú EF, Bercik P, Khan WI, Blennerhassett PA, Szechtman H, Collins SM.** Antidepressants attenuate increased susceptibility to colitis in a murine model of depression. *Gastroenterology* 130: 1743–1753, 2006.
23. **Wang LH, Fang XC, Pan GZ.** Bacillary dysentery as a causative factor of irritable bowel syndrome and its pathogenesis. *Gut* 53: 1096–1101, 2004.
24. **Zareie M, Johnson-Henry K, Jury J, Yang PC, Ngan BY, McKay DM, Soderholm JD, Perdue MH, Sherman PM.** Probiotics prevent bacterial translocation and improve intestinal barrier function in rats following chronic psychological stress. *Gut* 55: 1553–1560, 2006.

Available online at www.sciencedirect.com
ScienceDirect
Biochimica et Biophysica Acta 1778 (2008) 1035–1041
Biochimica et Biophysica Acta
BBA
www.elsevier.com/locate/bbamem

# Electrostatic interactions and complement activation on the surface of phospholipid vesicle containing acidic lipids: Effect of the structure of acidic groups

Keitaro Sou, Eishun Tsuchida *

*Research Institute for Science and Engineering, Waseda University, Tokyo 169-8555, Japan*

Received 5 September 2007; received in revised form 22 November 2007; accepted 7 January 2008
Available online 16 January 2008

**Abstract**

Anionic vesicles containing acidic phospholipids are known complement activators. To clarify which negative physicochemical electrostatic charges on vesicles and structural specificities of acidic lipids are critical to complement activation, the electrostatic properties and activity to complement of two anionic vesicles modified with a carboxylic acid derivative or a conventional acidic phospholipid were compared. Electrophoretic mobility measurements indicated that the negative zeta potential and the electrostatic interactivity of these two anionic vesicles were equal at pH 7.4. However, the infusion of vesicles containing acidic phospholipid induced significant complement activation, while vesicles containing the carboxylic acid derivative failed to activate complement. These results indicate that the negative charge on the surface of vesicles is not critical for the activation complement, suggesting that complement activation is specific to the structure of acidic groups. This finding is likely to be important to the design of anionic biointerfaces and may support the promising medical applications of this anionic vesicle modified with a carboxylic acid derivative.


*Keywords:* Liposome; Acidic lipid; Anionic surface; Electrostatic interaction; Complement activation

## 1. Introduction

Anionic vesicles (liposomes), commonly formulated by mixing acidic phospholipids such as phosphoglycerol, phosphoserin, phosphoinositol, phosphatidic acid, cardiolipin, and poly (ethylene glycol) (PEG) conjugated phosphoethanolamine in lipid components are known to mediate complement activation [1–5]. Complement activation, which is followed by systemic immune activation and anaphylaxis shock, is regarded as a critical problem in the clinical setting of various biomaterials. The C1q subcomponent of C1 has a highly cationic region in residues 14–26 of the C1qA polypeptide chain, and this specific region of the collagenous stalk of C1q has been identified as being involved in interactions with negatively charged activators [5–8]. It is believed that the antibody-independent binding of C1q to the negatively charged surface of vesicles initiates the activation of the complement cascade via the classical complement pathway [2]. To prevent complement activation, the acidic phospholipids can be removed or their negative charge can be protected by chemical modification [2,4]. It has also been reported that surface modification with a dense PEG layer is effective for preventing complement activation by covering the surface charge [9].

Our group has developed phospholipid vesicles called hemoglobin-vesicles that encapsulate human hemoglobin and that can be used as a substitute for red blood cells and as an alternative to conventional transfusion [10–14]. To achieve this challenging application of vesicles, we had to develop anionic vesicles capable of encapsulating hemoglobin using a minimum amount of lipids, retaining the negative charge on the membrane which reduces the lamellarity of vesicles and is required for improving encapsulation capacity [11–13]. Several acidic lipids have been tested and a carboxylic acid derivative, L-glutamic

* Corresponding author. Tel.: +81 3 5286 3120; fax: +81 3 3205 4740.
*E-mail addresses:* ksou@waseda.jp (K. Sou), eishun@waseda.jp (E. Tsuchida).

0005-2736/$ - see front matter © 2008 Elsevier B.V. All rights reserved.
doi:10.1016/j.bbamem.2008.01.006

acid, *N*-(3-carboxy-1-oxopropyl)-, 1,5-dihexadecyl ester (SA), has been used as an anionic component. Vesicles containing SA have been demonstrated to efficiently encapsulated hemoglobin, and given their stability, can be infused in considerably large doses as a red blood cell substitute [15,16]. In addition, administration of this formulation is not associated with considerable rejection by the blood immune system and complement in animals [17,18]. Recent collaboration involving our group found that vesicles containing SA are selectively captured by bone marrow macrophages at small injection doses in rabbits [19]. This targeting of bone marrow has not yet been reported for conventional anionic vesicles. These findings suggest that the surface characteristics of the anionic vesicles have a marked effect on their associated biological events and that this is highly dependent upon the nature of the acidic groups.

Based on the hypothesis that the negative electrostatic charge of acidic phospholipids on the surface of vesicles is one of the factors responsible for inducing complement activation, the electrostatics of vesicles containing SA may differ from those of vesicles containing acidic phospholipids. Conversely, when the electrostatic interactivity of these acidic lipids is equal, biological events such as complement activation are likely to be mediated by the molecular specificity of acidic lipids. To elucidate what aspects are critical to the biocompatibility and performance of anionic vesicles, a comparative analysis of the electrostatic interfacial properties of vesicles containing either SA or acidic phospholipids is essential. In this study, we elucidated the electrostatic interfacial properties of vesicles containing SA or an acidic phospholipid by electrophoretic mobility measurement and observed complement activation after the infusion of these vesicles in animals. The results clearly demonstrated that the negatively charged group on the surface of anionic vesicles is not critical to the activation of complement.

## 2. Materials and methods

### 2.1. Materials

1,2-Dipalmitoyl-*sn*-glycero-3-phosphocholine (PC), cholesterol (CH), and 1,2-dipalmitoyl-*sn*-glycero-3-phosphoglycerol (PG), and L-glutamic acid, *N*-(3-carboxy-1-oxopropyl)-, 1,5-dihexadecyl ester (SA), were purchased from Nippon Fine Chemical Co. Ltd. (Osaka, Japan). 1,2-Distearoyl-*sn*-glycero-3-phosphoethanolamine-*N*-[monomethoxy poly(ethylene glycol) (5000)] (PEG-DSPE) was purchased from NOF Co. (Tokyo, Japan). Pentalysine and poly-L-lysine (Mw. 15–30 kDa) were purchased from SIGMA (St. Louis, MO).

### 2.2. Preparation of vesicles

Vesicle samples were produced using PC and CH (1:1, molar ratio, PC-vesicles), and varying amounts of SA (SA-vesicles) or PG (PG-vesicles). The mixed lipids were added to 10 mM phosphate buffer (NaCl; 20 mM, pH 7.4) and the dispersion was introduced into an extruder (Lipex Biomembrane, Canada) and extruded through the membrane filters (final pore size: 0.2 μm, Isopore®, Millipore, Tokyo, Japan) under pressure using nitrogen gas. For animal experiments, vesicles were composed of PC, CH, and SA or PG (1:1:0.2, molar ratio), with 0.3 mol% of PEG-DSPE incorporated to prevent the aggregation of vesicles [20]. Samples for animal experiments were prepared under sterile conditions.

### 2.3. Characterization of vesicles

The diameters of the resulting vesicles were determined with a COULTER submicron particle analyzer (N4SD, Coulter, Hialeah, FL), and the average diameter ± standard deviation (SD) was calculated. The phospholipid concentration was determined using a cholineoxidase method (Phospholipid C Test Wako; Wako Pure Chem., Tokyo). Endotoxin contamination in the samples prepared for the animal experiment was determined to be less than 0.1 EU/mL by the Limulus assay test [21].

### 2.4. Determination of zeta potential

A 10 μL aliquot of vesicles (lipid concentration: 2 g/dL) was diluted in 2 mL of 10 mM phosphate buffer (pH 3–9, 37 °C) containing 20 mM NaCl and incubated for 1 h at 37 °C. The pH was determined using a pH meter with a pH electrode (F-52, HORIBA, Kyoto, Japan) at 37 °C and the electrophoretic mobility of vesicles (lipid concentration: 0.01 g/dL) were determined by Laser Doppler Velocimetry (Zeta-Sizer Nano ZS, Malvern Instruments, Malvern, Worcestershire, UK). Measurement conditions and parameters were as follows: 37 °C, dielectric constant 74.4 (for dilute water solution), viscosity 0.6864 cP (for dilute water solution), and the applied voltage was 20 V/cm. The zeta potential was determined by measuring the electrophoretic mobility ($U_E$), and the zeta potential ($\zeta$) and applied to the Henry equation:

$$U_E = \frac{2\varepsilon\zeta f(\kappa R)}{3\eta} \quad (1)$$

where $\varepsilon$ is the dielectric constant, $\eta$ is the viscosity of the solvent, $f(\kappa R)$ is the Henry function, $\kappa$ is the Debye–Hückel parameter and the $R$ is the radius of the particle. The Smoluchowski equation was used with $f(\kappa R) = 1.5$ employed in the zeta potential calculations. Measurements were performed four times for each sample and statistical analysis was conducted using the average ± SD of the four measurements.

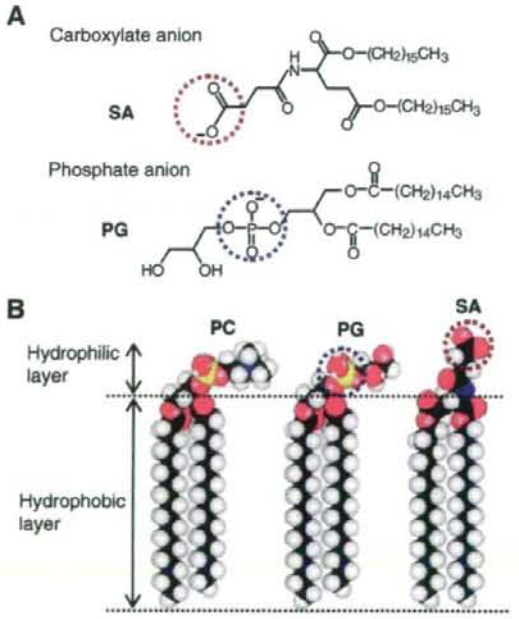


Fig. 1. Structure of acidic lipids for surface modification of vesicles. (A) Chemical structure of L-glutamic acid, *N*-(3-carboxy-1-oxopropyl)-, 1,5-dihexadecyl ester (SA) and 1,2-dipalmitoyl-*sn*-glycero-3-phosphoglycerol (PG). The focus of this study is the different acidic groups shown in the dotted circle. (B) The CPK model of SA and PG with 1,2-dipalmitoyl-*sn*-glycero-3-phosphocholine (PC) to estimate the distance of acidic groups from the membrane surface of PC. CPK models show the structure with minimized energy in molecular mechanistic calculation.

### 2.5. Electrostatic interactivity

The electrostatic interactivity of the anionic vesicles was evaluated using the change in the zeta potential in presence of $Ca^{2+}$, pentalysine, and poly-L-lysine (Mw. 15–30 kDa) as an index. A 10 μL aliquot of vesicles (lipid concentration: 2 g/dL) was diluted in 2 mL of 10 mM 2-[4-(2-Hydroxyethyl)-1-piperazinyl] ethanesulfonic acid (HEPES) buffer (pH 7.4, 37 °C) containing 0–3 mM $CaCl_2$ and 17–20 mM NaCl (total 20 mM), or containing varying amounts of pentalysine or poly-L-lysine (Mw. 15–30 kDa) with 20 mM NaCl. The dispersions were incubated for 1 h at 37 °C before mobility measurement of the vesicles was performed by electrophoresis as described in Section 2.4.

### 2.6. Animal experiments

Animal experiments were conducted under the guidelines recommended by the National Institutes of Health, Animal Use and Care and the protocol was approved by the Steering Committee for Animal Experimentation at Waseda University. Male Wistar rats (250±20 g) were anesthetized with ether. The vesicular dispersion (5 g/dL) was introduced into rats through the tail veins at 1 mL/min ($n$=5 for each sample). Each rat received 5.6 mL/kg of body weight of vesicle dispersion (lipids: 280 mg/kg of body weight). At 1 or 24 h after injection, the blood was collected and centrifuged to separate the serum ($1\times10^3$ g, 10 min). The collected serum was further ultracentrifuged to remove the vesicles ($3\times10^5$ g, 30 min). The 50% hemolytic unit of complement serum (CH50) was determined in accordance with general procedures for clinical laboratory tests by a commercial company (BML, Japan).

### 2.7. Statistical methods

The data from the animal experiments are reported as means±standard error of the mean. Statistical analysis was performed using Microsoft Excel for Windows and CH50 values were compared using Student's unpaired t test.

## 3. Results and discussion

### 3.1. Samples

Two characteristic acidic lipids used in this study are shown in Fig. 1. SA and PG each have carboxylic acid and phosphoric acid as ionized groups, respectively. Both lipids have a strongly hydrophobic dialkyl structure to fix the ionized groups on vesicle surface. The molecular length indicated by the CPK model showed that the carboxylate anion of SA and the phosphate anion of PG would be located at the surface of PC-vesicles (Fig. 1B). Various amounts of SA and PG were incorporated into the PC/CH membrane (1:1, molar ratio) of the anionic vesicles. The size of vesicles was controlled by extrusion methods (final pore size: 0.2 μm), with final mean diameters of approximately 200 nm (Table 1). The vesicles prepared without acidic lipids or with 1 mol% of acidic lipids tended to be slightly larger (ca 30 nm) than vesicles containing more acidic lipids. This effect of acidic lipids on the size of vesicles could be due to the improved dispersion stability of vesicles and electrostatic repulsion of the anionic surfaces. The vesicles without acidic lipids were observed to precipitate in a day, indicating poor dispersion stability. Vesicles without acidic lipids containing small amount of PEG-DSPE to prevent aggregation had diameters of 202±49 nm. Therefore, the slightly large diameter of vesicles without acidic lipids or with 1 mol% of acidic lipids may be the cause for their increased aggregability. The low aggregability of vesicles having large zeta potential is due to their electrostatic repulsive interaction causing anionic vesicles to exist as stable dispersions.

Table 1
Diameter of prepared vesicles containing various amounts of acidic lipid

| Acidic lipid (mol%) | Mean diameter±SD (nm) | |
|---|---|---|
| | SA-vesicles | PG-vesicles |
| 0 (PC-vesicles) | 232±60 | 232±60 |
| 1 | 224±58 | 230±60 |
| 5 | 193±50 | 196±58 |
| 9 | 205±40 | 204±49 |
| 15 | 194±45 | 199±55 |
| 20 | 198±52 | 194±64 |

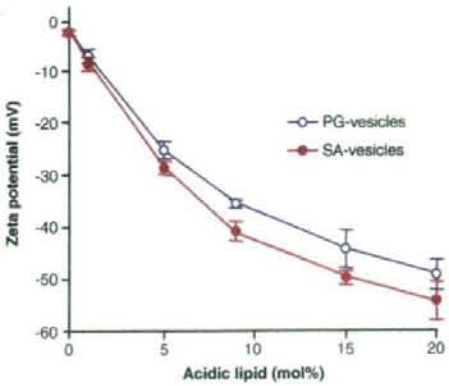


Fig. 2. Zeta potential of vesicles modified with SA (SA-vesicles) and PG (PG-vesicles) as a function of acidic lipid content. Zeta potentials were measured in 10 mM phosphate buffer (pH 7.4, NaCl; 20 mM) at 37 °C.

### 3.2. Zeta potential of vesicles

The zeta potential is the electrostatic potential at the hydrodynamic slip plane, and is characterized as having an electrical double-layer consisting of the Stern layer and the diffuse layer. Fig. 2 shows the zeta potential of prepared vesicles as a function of acidic lipid content at pH 7.4. Vesicles containing PC/CH (1:1, molar ratio) have an almost neutral surface (zeta potential: −2.22±0.62 mV), indicating that the surface is inactive for electrostatic events. The magnitude of the negative charge on the surface increased with the incorporation of SA or PG, indicating that the ionized groups of SA and PG act to characterize the vesicle surface depending on their content. The zeta potentials of SA-vesicles and PG-vesicles reached −54.2±3.68 mV and −49.0±2.89 mV for acidic lipids of 20 mol%, respectively, with the negative zeta potential of SA-vesicles being relatively higher compared to that of PG-vesicles at any concentration. In theory, the electrostatic potential is dependent upon distance from the membrane surface as well as surface charge density [22]. The slightly extended negative charge of SA from the surface shown in Fig. 1B, would reduce the distance between the change to slip plane, resulting in the higher negative zeta potential of SA-vesicles.

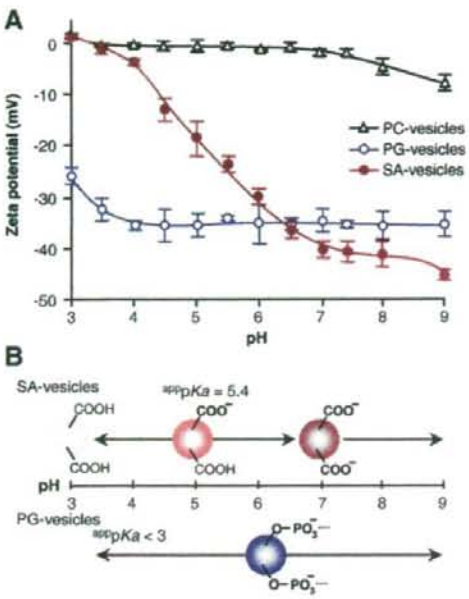


Fig. 3. Ionization state of acidic groups as a function of pH. (A) Zeta potential of vesicles (PC/CH, 1:1, molar ratio) (PC-vesicles), and vesicles containing 9 mol% of SA (SA-vesicles) or PG (PG-vesicles) at various pH. Zeta potentials were measured in 10 mM phosphate buffer (NaCl; 20 mM) at various pH (37 °C). (B) Schematic representation of the ionization state of acidic groups with pH. The apparent $pK_a$s of SA-vesicles and PG-vesicles were calculated to be 5.4 and <3.

This result demonstrated that the capacity of SA as an anionic component of vesicles is equal to acidic phospholipids at pH 7.4.

### 3.3. Ionization properties of acidic lipids

Stability of the ionization state conferred by acidity is an important characteristic of acidic compounds. We examined the ionization properties of acidic lipids as a function of pH using SA-vesicles and PG-vesicles containing acidic lipids of 9 mol% with zeta potentials of −40.7±2.09 mV and −35.4±0.61 mV (at pH 7.4), respectively. As shown in Fig. 3A, the zeta potential of SA-vesicles varied markedly depending on the environmental pH (pH 3–7). The change in the zeta potential of SA-vesicles is thought to reflect the ionization state of SA, as control vesicles without SA, namely PC-vesicles, maintained almost neutral surfaces irrespective of pH. The relationship between pH and the $pK_a$ of the acid is expressed using the well-known Henderson–Hasselbalch equation as follows:

$$\mathrm{pH} = \mathrm{p}K_a + \log\frac{[-\mathrm{COO}^-]}{[-\mathrm{COOH}]}. \quad (2)$$

When we analyzed the data shown in Fig. 3A using Eq. (2) and the assumption that the zeta potential was linearly correlated with the ionization acid, the $pK_a$ of the carboxyl group of SA was estimated as 5.4 (Fig. 3B). Above pH 7, the zeta potential of SA-vesicles was almost constant, indicating that the carboxyl group of SA would mostly be ionized above pH 7. The zeta potentials of PG-vesicles were almost constant in the range pH 4–9, indicating that the ionized form of the phosphoric acid moiety is stable in this range. The change in the zeta potential observed at a pH lower than pH 4, and its $pK_a$ would be lower than pH 3 [23,24]. Thus, we confirmed that the surface of SA-vesicles and PG-vesicles exhibited the characteristics of a weak acid with SA and a strong acid with PG, respectively, indicating that the individual characteristics of acidic groups are expressed on the surface of vesicles. We also observed that the magnitude of the negative electrostatic charges in SA-vesicles was equal to that observed in PG-vesicles at approximately neutral pH.

### 3.4. Electrostatic interactivity

$Ca^{2+}$ is found in biological fluids (normally 2–3 mM in plasma) and is known to mediate biological processes by binding to the anionic domains such as those involved in the specific binding of proteins to membranes [25,26]. Acidic phospholipids, such as PG and PS, are also known to bind $Ca^{2+}$ [27–29]. As shown in Fig. 4, the negative charge on anionic vesicles was suppressed by increasing the concentration of $Ca^{2+}$. When the concentration of $Ca^{2+}$ was increased to 3 mM, the zeta potentials of SA-vesicles and PG-vesicles were −16.4±1.9 mV and −13.8±1.4 mV, respectively. Recently, Hautala et al. reported that vesicles containing phosphatidic acid possess a specifically strong affinity for $Ca^{2+}$, and that the zeta potential of these vesicles changed from being strongly negative to positive after binding $Ca^{2+}$ [29]. These authors also showed that other acidic phospholipids, including PG, do not exhibit a strong affinity towards becoming cationic. Consequently, one aim of this experiment was to determine whether the binding of $Ca^{2+}$ is a specificity factor between SA-vesicles and PG-vesicles, and also whether the surface of SA-vesicles remained negative in the presence of $Ca^{2+}$. Our experiment showed that the surface of the SA-vesicles remained

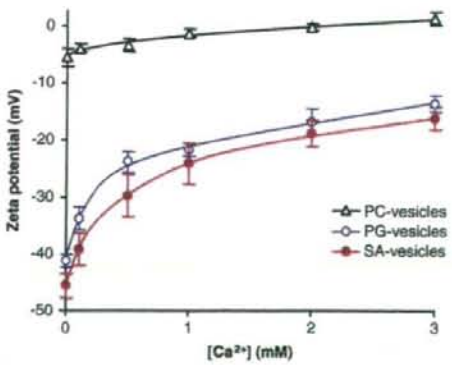


Fig. 4. Change in zeta potential of vesicles as a function of $Ca^{2+}$ concentration. Vesicles were dispersed at 100 μg/mL in 10 mM HEPES buffer (pH 7.4, at 37 °C) containing NaCl and $CaCl_2$ (total: 20 mM). PC-vesicles: PC/ CH (1:1, molar ratio), SA-vesicles: PC/CH/SA (1:1:0.2, molar ratio), and PG-vesicles: PC/CH/PG (1:1:0.2, molar ratio).

negative in the presence of $Ca^{2+}$. In addition, comparisons of SA-vesicles and PG-vesicles also showed that the specificity of binding $Ca^{2+}$ was not observed.

Additional model-based studies of electrostatic interactivity, pentalysine and poly-L-lysine (Mw. 15–30 kDa with a repeating primary lysine amine) were also conducted. Oligomers or polymers of lysine are often used to model basic peptides or macromolecules and their electrostatic interactions on membranes [30,31]. As shown in Fig. 5, the zeta potential is a linear function of the concentration of pentalysine. The lines, which represent the least-squares best fit, have slopes of 9.3 and 7.4 mV per decade for the pentalysine concentrations in SA-vesicles and PG-vesicles. The slope for PC-vesicles was as little as 0.26 mV per decade of pentalysine concentration (data not shown), indicating that the negative charge of acidic lipids mediate the interaction with basic pentalysine. A change in the zeta potential is due to binding of basic peptide [31] and a similar decay slope of the zeta potential would indicate that the binding constant of a basic peptide to SA-vesicles and PG-vesicles was similar. As shown in Fig. 6, the change in the zeta potential of these vesicles due to the interaction with poly-L-lysine increased drastically, changing from a negative to a positive in presence of 1.5–2 μg/mL poly-L-lysine. Conversely, the change in the surface potential of PC-vesicles was negligible, indicating that the acidic lipids mediate the interaction with basic macromolecules. This experiment also demonstrates that the interactivity of SA-vesicles and PG-vesicles to basic macromolecules is equal at pH 7.4, and that within an electrostatic context, SA-vesicles and PG-vesicles interact similarly with basic compounds at physiological pH. It has been shown that electrostatic interactions are involved in the binding of C1q to the surface of anionic vesicles containing acidic phospholipid [6]. In the event that the negative charge on the surface of vesicles is critical for complement activation, both the SA-vesicles and PG-vesicles should be capable of activating the complement system to similar degree. We therefore conducted animal experiments to clarify the issue of complement activation by the anionic electrostatic charge of vesicles.

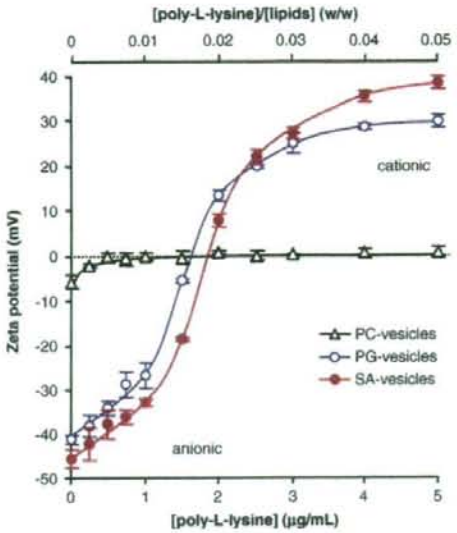


Fig. 6. Change in zeta potential of vesicles as a function of the concentration of basic macromolecule (poly-L-lysine, Mw. 15–30 kDa). Vesicles were dispersed at 100 μg/mL in 10 mM HEPES buffer (pH 7.4, at 37 °C, NaCl, 20 mM) containing various amount of poly-L-lysine. PC-vesicles: PC/CH (1:1, molar ratio), SA-vesicles: PC/CH/SA (1:1:0.2, molar ratio), and PG-vesicles: PC/CH/PG (1:1:0.2, molar ratio).

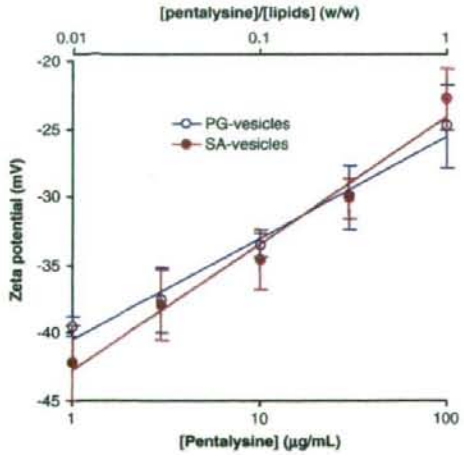


Fig. 5. Change in zeta potential of vesicles as a function of the concentration of basic oligomer (pentalysine). Vesicles were dispersed at 100 μg/mL in 10 mM HEPES buffer (pH 7.4, at 37 °C, NaCl, 20 mM) containing various amount of pentalysine. The lines have slopes of 9.3 and 7.4 mV per decade for the pentalysine concentrations in SA-vesicles and PG-vesicles. SA-vesicles: PC/CH/SA (1:1:0.2, molar ratio) and PG-vesicles: PC/CH/PG (1:1:0.2, molar ratio).

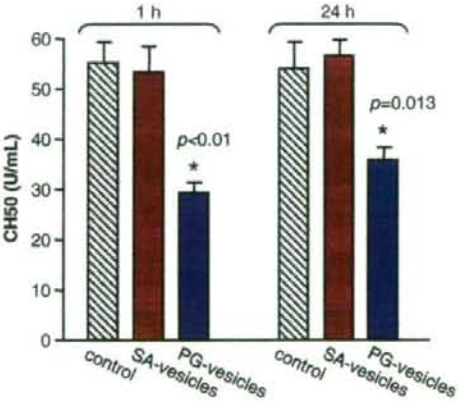


Fig. 7. Comparison of the 50% hemolytic unit of complement (CH50) in rat serum at 1 or 24 h after infusion of saline (control), SA-vesicles, or PG-vesicles. CH50 value for PG-vesicles was significantly lower than that of the control ($p<0.01$ at 1 h, $p=0.013$ at 24 h), indicating the complement consumption in serum after activation. Equal CH50 value for SA-vesicles with the control indicates that SA-vesicles failed to activate complement.

### 3.5. Complement activation

Serum was collected at 1 and 24 h after the infusion of SA-vesicles or PG-vesicles in experimental rats to determine CH50 levels. The control group received saline as a vehicle. The values of CH50 in control rats, and SA-vesicles- and PG-vesicles-administered rats, were 55.1±4.1 U/mL, 53.2±4.8 U/mL, and 29.3±1.6 U/mL at 1 h after infusion of sample, respectively. At 24 h, the values of CH50 in control rats, and SA-vesicles- and PG-vesicles-administered rats, were 54.0±4.7 U/mL, 56.5±3.3 U/mL, and 35.8±2.3 U/mL, respectively (Fig. 7). The lower CH50 levels observed in the PG-vesicles-administered group in comparison with the control group indicate that complement consumption occurred after activation. These findings imply that significant complement activation is induced in rats receiving PG-vesicles compared to the control group ($p<0.01$ at 1 h, $p=0.013$ at 24 h). Complement consumption was not observed in rats administered SA-vesicles.

Since the negative charge and electrostatic interactivity of SA-vesicles were the same as in PG-vesicles (Figs. 2–6), the data obtained from the animal experiments indicates that the negative charge on the anionic vesicle is not a critical factor underlying the activation of complement. The first step in the activation of the classical complement pathway involves the binding of an activator to C1q, resulting in the activation of serine proteases C1r and C1s. It has been suggested that the negative charge of an activator such as PG-vesicles is involved in some way with the binding of the activator to C1q [1–8]. Assuming that the electrostatic interaction is non-specific, SA-vesicles should interact with C1q electrostatically. Since the action of complement proteases, which follows the binding of the activator to the C1q, is known to be highly specific [32,33], it seems likely that complement activation on anionic surface is limited to an activation step rather than a binding step. Such specific activation of complement by the anionic vesicles in the present study may be involved in the physiological regulation of complement activation on anionic biomembranes.

## 4. Conclusions

The carboxylic acid of SA and phosphoric acid of PG have equal capacity as anionic components of vesicles at neutral pH. The results presented in this investigation demonstrated that the negative electrostatic charge of anionic vesicles is not a critical factor in the activation of complement. Rather, the induction of complement activation by anionic vesicles is dependent on the structure of acidic lipids. This finding may facilitate development and various biological applications of anionic vesicles.

## Acknowledgements

This work was partly supported by Health Sciences Research Grants (Research on Regulatory Science); the Ministry of Health, Labour and Welfare, Japan, and the Ministry of Education, Science, Sports and Culture, Grant-in-Aid for Scientific Research (B), 17300162. The authors gratefully acknowledge Dr. K. Kobayashi and Dr. H Horinouchi (Keio University) for their support in the animal experiments, Dr. M. Suematsu (Keio University) for an important suggestion on bioactivity of anionic vesicles, and Dr. S. Takeoka and Dr. H. Sakai (Waseda University) for advice and discussions related to this research.

## References

[1] H.C. Loughrey, M.B. Bally, L.M. Reinish, P.R. Cullis, The binding of phosphatidylglycerol liposomes to rat platelets is mediated by complement, Thromb. Haemost. 64 (1990) 172–176.
[2] A. Chonn, P.R. Cullis, D.V. Devine, The role of surface charge in the activation of the classical and alternative pathways of complement by liposomes, J. Immunol. 146 (1991) 4234–4241.
[3] J. Szebeni, The interaction of liposomes with the complement system, Crit. Rev. Ther. Drug Carr. Syst. 15 (1998) 57–88.
[4] S.M. Moghimi, I. Hamad, T.L. Andresen, K. Jorgensen, J. Szebeni, Methylation of the phosphate oxygen moiety of phospholipid-methoxy (polyethylene glycol) conjugate prevents PEGylated liposome-mediated complement activation and anaphylatoxin production, FASEB J. 20 (2006) 2591–2593.
[5] A.J. Bradley, D.E. Brooks, R. Norris-Jones, D.V. Devine, C1q binding to liposomes is surface charge dependent and is inhibited by peptides consisting of residues 14–26 of the human C1qA chain in a sequence independent manner, Biochim. Biophys. Acta 1418 (1999) 19–30.
[6] A.J. Bradley, E. Maurer-Spurej, D.E. Brooks, D.V. Devine, Unusual electrostatic effects on binding of C1q to anionic liposomes: role of anionic phospholipid domains and their line tension, Biochemistry 38 (1999) 8112.
[7] H. Jiang, B. Cooper, F.A. Robey, H. Gewurz, DNA binds and activates complement via residues 14–26 of the human C1q A chain, J. Biol. Chem. 267 (1992) 25597–25601.
[8] H. Jiang, D. Burdick, C.G. Glabe, C.W. Cotman, A.J. Tenner, beta-Amyloid activates complement by binding to a specific region of the collagen-like domain of the C1q A chain, J. Immunol. 152 (1994) 5050–5059.
[9] A.J. Bradley, D.V. Devine, S.M. Ansell, J. Janzen, D.E. Brooks, Inhibition of liposome-induced complement activation by incorporated poly(ethylene glycol)-lipids, Arch. Biochem. Biophys. 357 (1998) 185–194.
[10] E. Tsuchida (Ed.), Substitute: Present and Future Perspective, Elsevier Science, Amsterdam, 1998.
[11] S. Takeoka, T. Ohgushi, K. Terase, T. Ohmori, E. Tsuchida, Layer-controlled hemoglobin vesicles by interaction of hemoglobin with a phospholipid assembly, Langmuir 12 (1996) 1755–1759.
[12] H. Sakai, K. Hamada, S. Takeoka, H. Nishide, E. Tsuchida, Physical properties of hemoglobin vesicles as red cell substitutes, Biotechnol Prog. 12 (1996) 119–125.
[13] K. Sou, Y. Naito, T. Endo, S. Takeoka, E. Tsuchida, Effective encapsulation of proteins into size-controlled phospholipid vesicles using freeze-thawing and extrusion, Biotechnol Prog. 19 (2003) 1547–1552.
[14] H. Sakai, H. Horinouchi, M. Yamamoto, E. Ikeda, S. Takeoka, M. Takaori, E. Tsuchida, K. Kobayashi, Acute 40 percent exchange-transfusion with hemoglobin-vesicles (HbV) suspended in recombinant human serum albumin solution: degradation of HbV and erythropoiesis in a rat spleen for 2 weeks, Transfusion 46 (2006) 339–347.
[15] H. Sakai, Y. Masada, H. Horinouchi, E. Ikada, K. Sou, S. Takeoka, M. Suematsu, M. Takaori, K. Kobayashi, E. Tsuchida, Physiological capacity of the reticuloendothelial system for the degradation of hemoglobin vesicles (artificial oxygen carriers) after massive intravenous doses by daily repeated infusions for 14 days, J. Pharmacol. Exp. Ther. 311 (2004) 874–884.
[16] K. Sou, R. Klipper, B. Goins, E. Tsuchida, W.T. Phillips, Circulation kinetics and organ distribution of Hb-vesicles developed as a red blood cell substitute, J. Pharmacol. Exp. Ther. 312 (2005) 702–709.
[17] H. Abe, M. Fujihara, H. Azuma, H. Ikeda, K. Ikebuchi, S. Takeoka, E. Tsuchida, H. Harashima, Interaction of hemoglobin vesicles, a cellular-type artificial oxygen carrier, with human plasma: effects on coagulation, kallikrein-kinin, and complement systems, Artif. Cells Blood Substit. Biotechnol. 34 (2006) 1–10.

[18] H. Abe, H. Azuma, M. Yamaguchi, M. Fujihara, H. Ikeda, H. Sakai, S. Takeoka, E. Tsuchida, Effects of hemoglobin vesicles, a liposomal artificial oxygen carrier, on hematological responses, complement and anaphylactic reactions in rats, Artif. Cells Blood Substit. Biotechnol. 35 (2007) 157–172.
[19] K. Sou, B. Goins, S. Takeoka, E. Tsuchida, W.T. Phillips, Selective uptake of surface-modified phospholipid vesicles by bone marrow macrophages in vivo, Biomaterials 28 (2007) 2655–2666.
[20] K. Sou, T. Endo, S. Takeoka, E. Tsuchida, Poly(ethylene glycol)-modification of the phospholipid vesicles by using the spontaneous incorporation of poly (ethylene glycol)-lipid into the vesicles, Bioconjug. Chem. 11 (2000) 372–379.
[21] H. Sakai, S. Hisamoto, I. Fukutomi, K. Sou, S. Takeoka, E. Tsuchida, Detection of lipopolysaccharide in hemoglobin-vesicles by Limulus amebocyte lysate test with kinetic-turbidimetric gel clotting analysis and pretreatment of surfactant, J. Pharm. Sci. 93 (2004) 310–321.
[22] S. McLaughlin, The electrostatic properties of membranes, Annu. Rev. Biophys. Biophys. Chem. 18 (1989) 113–136.
[23] A. Watts, K. Harlos, W. Maschke, D. Marsh, Control of the structure and fluidity of phosphatidylglycerol bilayers by pH titration, Biochim. Biophys. Acta 510 (1978) 63–74.
[24] J.F. Tocanne, J. Teissié, Ionization of phospholipids and phospholipid-supported interfacial lateral diffusion of protons in membrane model systems, Biochim. Biophys. Acta 1031 (1990) 111–142.
[25] J. Rizo, T.C. Sudhof, C2-domains, structure and function of a universal $Ca^{2+}$-binding domain, J. Biol. Chem. 273 (1998) 15879–15882.
[26] J.E. Murphy, D. Tacon, P.R. Tedbury, J.M. Hadden, S. Knowling, T. Sawamura, M. Peckham, S.E. Phillips, J.H. Walker, S. Ponnambalam, LOX-1 scavenger receptor mediates calcium-dependent recognition of phosphatidylserine and apoptotic cells, Biochem. J. 393 (2006) 107–115.
[27] A. Lau, A. McLaughlin, S. McLaughlin, The adsorption of divalent cations to phosphatidylglycerol bilayer membranes, Biochim. Biophys. Acta 645 (1981) 279–292.
[28] C.G. Sinn, M. Antonietti, R. Dimova, Binding of calcium to phosphatidylcholine-phosphatidylserine membranes, Colloids and Surfaces A: Physicochem. Eng. Aspects 282–283 (2006) 410–419.
[29] J.T. Hautala, M.L. Riekkola, S.K. Wiedmer, Anionic phospholipid coatings in capillary electrochromatography. Binding of $Ca^{2+}$ to phospholipid phosphate group, J. Chromatogr. A 1150 (2007) 339–347.
[30] D. Volodkin, V. Ball, P. Schaaf, J.C. Voegel, H. Mohwald, Complexation of phosphocholine liposomes with polylysine. Stabilization by surface coverage versus aggregation, Biochim. Biophys. Acta 1768 (2007) 280–290.
[31] D. Murray, A. Arbuzova, G. Hangyás-Mihályné, A. Gambhir, N. Ben-Tal, B. Honig, S. MaLaughlin, Electrostatic properties of membranes containing acidic lipids and adsorbed basic peptides: theory and experiment, Biophys. J. 77 (1999) 3176–3188.
[32] G.J. Arlaud, C. Gaboriaud, N.M. Thielens, M. Budayova-Spano, V. Rossi, J.C. Fontecilla-Camps, Structural biology of the C1 complex of complement unveils the mechanisms of its activation and proteolytic activity, Mol. Immunol. 39 (2002) 383–394.
[33] G. O'Brien, N.S. Quinsey, J.C. Whisstock, R.N. Pike, Importance of the prime subsites of the C1s protease of the classical complement pathway for recognition of substrates, Biochemistry 42 (2003) 14939–14945.

# Structure, Photophysical Property, and Cytotoxicity of Human Serum Albumin Complexed with Tris(dicarboxymethylene)[60]fullerene

Xue Qu,[†] Teruyuki Komatsu,*[,†,‡] Takaaki Sato,[†] Otto Glatter,[§] Hirohisa Horinouchi,[||] Koichi Kobayashi,[||] and Eishun Tsuchida*[,†]

Research Institute for Science and Engineering, Waseda University, 3-4-1 Okubo, Shinjuku-ku, Tokyo 169-8555, Japan, PRESTO, Japan Science and Technology Agency (JST), Institute of Chemistry, University of Graz, Heinrichstrasse 28, A-8010 Graz, Austria, and Department of Thoracic Surgery, School of Medicine, Keio University, 35 Shinanomachi, Shinjuku-ku, Tokyo 160-8582. Received February 6, 2008; Revised Manuscript Received June 18, 2008

We present structure, photoexcited triplet-state property, and singlet oxygen ($^1O_2$) generation capability of human serum albumin complexed with a tris(dicarboxymethylene)[60]fullerene $C_3$-isomer (HSA−CF). Small angle X-ray scattering measurements showed that a globular size-dimension and surface charge distribution of HSA were unaltered by monomolecular complexation of CF into the hydrophobic cavity. Laser flash photolysis to the HSA−CF solution yielded a photoexcited triplet state of the CF chromophore ($^3$CF*) with lifetime of 46 $\mu$s. In the presence of $O_2$, energy transfer occurred from HSA−$^3$CF* to $O_2$ to generate $^1O_2$; the quenching rate constant [$k_q(O_2)$] was determined to be $2.2 \times 10^8$ $M^{-1}$ $s^{-1}$. The HSA−CF showed strong photoresistence relative to HSA complexed with a protoporphyrin IX. The quantum yield of $^1O_2$ production for this artificial protein was compared to those of other photosensitizing agent. The HSA−CF did not show a dark cytotoxicity, but induced cell death efficiently under visible light irradiation.

## INTRODUCTION

Photodynamic therapy (PDT) is a nonsurgical cancer treatment that combines a photosensitizing medication with exposure to visible light (*1, 2*). Highly cytotoxic singlet oxygen ($^1O_2$) formed by energy transfer from photoexcited sensitizer to molecular $O_2$ has been implicated as an intermediary species leading to cell death in tumors. To accelerate this $^1O_2$ generation, a range of organic dyes, especially porphyrin compounds, have been synthesized as photosensitizers (*3*). The most widely used reagent in clinical PDT is Photofrin, which is a heterogeneous mixture of hematoporphyrin oligomers (*1, 2, 4*). Several porphyrin or chlorin derivatives are also being tested as second generation (*1, 2, 5, 6*). Another well-known agent approved by the FDA is Levulan; 5-aminolevulinic acid (ALA) (*7–9*). ALA-induced photosensitization is unique approach that utilizes the heme biosynthetic pathway to produce endogenous protoporphyrin IX (PP). When ALA enters cancer cells, it triggers the synthesis of PP, which acts as an active sensitizer. Wavelengths typically used in PDT are between 600 and 800 nm, because light below 600 nm is absorbed by tissues and hemoglobin (Hb). Photofirin is normally excited by a red light (630 nm) using an Excimer dye-laser (*1, 2*). The ALA-PDT also uses the 630 nm laser, while the irradiation using a metal halide lamp or xenon arc lamp is still popular, because this is reasonable in comparison to the expensive laser pulse system and suitable for irradiation of the wide area of the diseased part (*9*). In fact, the light source approved in the U.S. for ALA-PDT was halogen lamp ($\lambda_{exc}$ = 410 nm). Buckminster[60]fullerene ($C_{60}$) produces $^1O_2$ by energy transfer with extremely high quantum yield ($\Phi_\Delta$: 0.96, $\lambda_{exc}$ = 532 nm) (*10, 11*) and generally shows strong photoresistance compared to the porphyrins. Consequently, various water-soluble fullerenes and fullerene−polymer hybrids have been prepared as a new class of photosensitizer for $^1O_2$ production (*11–16*). However, we would like to emphasize herein that most exogenous compounds administered into our bloodstream are immediately captured by human serum albumin (HSA, Mw: 66.5 kDa), which is the major protein component in our blood plasma (*17, 18*). To evaluate the biological performance of the fullerene, we must investigate the structure and function of the HSA−fullerene complex. Despite that necessity, photochemistry of the HSA−fullerene complex has never been studied to date. In this paper, we report for the first time the structure and photoexcited triplet-state properties of HSA complexed with a tris(dicarboxymethylene)[60]fullerene $C_3$-isomer (HSA−CF) and highlight its photoinduced energy transfer to $O_2$ to produce $^1O_2$. Furthermore, cytotoxicity of HSA−CF in vitro has also been evaluated. It is known that CF acts as a neuroprotective agent (*19*) and binds to HSA (*20*), but its photophysical behavior and cytotoxicity under visible light irradiation have not been elucidated.

## EXPERIMENTAL PROCEDURES

**Materials and Apparatus.** All reagents were purchased from commercial sources as special grades and used without further purification. Recombinant HSA expressed in *Pichia pastoris* was purchased from Sigma-Aldrich Corp. Tris(dicarboxymethylene)-[60]fullerene $C_3$-isomer (CF) was purchased from Axxora LLC and 2-[4-(2-hydroxyethoxy)phenyl]-1,3-dioxolo-4*a*,5*a*-[60]fullerene (HF) was purchased from FLOX Corp. Protoporphyrin IX (PP), protoporphyrin IX dimethyl ester (PPDME), and [60]fullerene ($C_{60}$) were purchased from Sigma-Aldrich Corp. The water was deionized using a Millipore Elix and Simpli Laboratory-UV. The UV−vis absorption spectra for the potassium phosphate buffered (PB) solution (pH 7.0, 50 mM) of the HSA−fullerene complex (normally 20 $\mu$M) were recorded using an Agilent 8453 UV−visible spectrophotometer with an Agilent

* Corresponding author. (E.T.) Tel: +81-3-5286-3120, Fax: +81-3-3205-4740, E-mail: eishun@waseda.jp. (T.K.) E-mail: teruyuki@waseda.jp.
[†] Waseda University.
[‡] PRESTO, JST.
[§] University of Graz.
[||] Keio University.

10.1021/bc800207j CCC: $40.75 
Published on Web 07/22/2008

89090A temperature control unit. The CD spectra for the PB solution of the HSA−fullerene complex were measured using a JASCO J-820 circular dichrometer. The concentration of the HSA sample was 2 $\mu$M and a quartz cuvette with a 2.0 mm thickness was used for measurements in the range 195−250 nm. Mass spectroscopic analyses were performed using a JEOL JMS-T100CS ESI-TOF mass spectrometer.

**Preparations of HSA−Fullerene Complexes.** Typically, 3.92 mL of a PB solution (pH 7.0, 50 mM) of HSA (0.25 mM) was mixed with 1.0 mL of 0.98 mM CF in PB (CF/HSA molar ratio of 1:1) and incubated for 12 h with rotation in the dark at room temperature. The complex was then diluted with 50 mM PB solution and concentrated to the initial volume using a Vivaspin 20 centrifuge filter (5 kDa MW cutoff) at 4000 × $g$ using a Beckman Coulter Allegra X-15R centrifuge. In the case of HSA−HF, 4.29 mL of PB solution (pH 7.0, 50 mM) of HSA (42 $\mu$M) was mixed with 0.67 mL of 0.267 mM HF in DMSO (HF/HSA molar ratio of 1:1) and incubated for 12 h with rotation in the dark at room temperature ([DMSO] = 13.5 vol %). The complex was then diluted using 50 mM PB solution and concentrated to the initial volume using a Vivaspin 20 centrifuge filter at 4000 × $g$. These dilution/concentration cycles were repeated to reduce the DMSO concentration to <0.1 vol %. The obtained protein solution was loaded on a Superdex 75 g gel-permeation column by elution of 50 mM PB using an ÄKTA Prime Plus FPLC system; only one band was observed during the chromatography. The PB solutions (pH 7.0, 50 mM) of HSA−CF and HSA−HF ([HSA]: 20 $\mu$M) in a 10-mm-path length optical quartz cuvette sealed with a rubber septum was degassed and purged using $N_2$ prior to use. The HSA complexed with PP (HSA−PP) was also prepared by the same procedure as HSA−HF.

**HPLC.** HPLC measurement of the HSA−fullerene complex was carried out using an HPLC system consisted of a Shimadzu LC-8A pump and a Shimadzu SPD-10A UV detector. A Shodex Protein KW-803 column was used with PB (pH 7.0, 10 mM) as the mobile phase at 22 °C (1.0 mL $min^{-1}$).

**Isoelectric Focusing (IEF).** The IEF was performed using an Amersham Biosciences Electrophoresis Power Supply EPS 301 with an Invitrogen Novex pH 3−7 IEG Gel. The protein marker used was a GE Healthcare IEF calibration kit Low Range $p$I (pH 2.5−6.5). The voltage was gradually raised to 300 V for 4 h. The gels were stained by a Daiichi Pure Chemicals PAGE Blue 83 and distained by washing with aqueous ethanol/acetic acid and 10% acetic acid.

**Small-Angle X-ray Scattering (SAXS).** SAXS experiments were carried out using an Anton Paar SAXSess camera in the $q$-range 0.10−9.0 $nm^{-1}$. Deionization of the protein sample was performed by dilution/concentration cycles with pure water using Vivaspin 20 centrifuge filter (5 kDa MW cutoff) at 4000 × $g$, giving an aqueous solution of the HSA−CF complex. Washing with phosphate buffered saline (PBS) solution (pH 7.4, 150 mM) gave the PBS solution of the protein. The scattered intensity $I(q)$ was generally given as $I(q) = nP(q)S(q)$ for globular particle system, where $n$ is the particle number density, $P(q)$ is the form factor, and $S(q)$ is static structure factor. The measured intensities were normalized to give the uniform primary intensity at $q$ = 0 and converted into absolute scale using water as a secondary standard. A model-independent collimation-correction procedure was made via an indirect Fourier transformation (IFT) technique. The pair-distance distribution functions $p(r)$ of HSA and HSA−CF in solution, which are given as inverse Fourier transformations of the form factor $P(q)$ into real space, were obtained using IFT technique for a highly diluted sample ($S(q)$ ~ 1) and its generalized version (GIFT) for $c$ > 1 g $dL^{-1}$. The GIFT technique enables splitting of $I(q)$ into $P(q)$ and $S(q)$, letting $P(q)$ and the resulting $p(r)$ virtually model free, where we assumed a screened Coulomb (Yukawa) potential and Rogers-Young (RY) closure relation. We made a complementary analysis to deduce the experimental structure factor, $S(q)^{exp}$, by dividing the normalized intensity $I(q)/c$ by the experimental form factor $P(q)^{exp}$ determined at very low concentration, which confirms the validity of the GIFT results.

**Laser Flash Photolysis.** The transient absorption spectra and triplet lifetime measurements were carried out using a Unisoku TSP-1000WK time-resolved spectrophotometer with a Spectron Laser Systems SL803G-10 Q-switched Nd:YAG laser, which generated a second-harmonic (532 nm) pulse of 6 ns duration (10 Hz) (*21*). The samples (20 $\mu$M) of the PB solutions (50 mM, pH. 7.0) of HSA−CF, HSA−HF, HSA−PP, THF solution of PPDME, and toluene solution of $C_{60}$ were held in a quartz cuvette (optical path length; 10 mm); experiments were carried out at 22 °C. The gas mixture with the desired partial pressure of $O_2/N_2$ prepared by a KOFLOC Gasbrender GB-2C was flowed into the sample cuvette for 20 min for equilibration.

**Near-Infrared Photo-Counting Measurement.** The emission spectrum of $^1O_2$ ($^1\Delta_g \rightarrow {}^3\Sigma_g^-$) was measured using a Hamamatsu Photonics C8282W Near-Infrared Photo-Counting System equipped with a Hamamatsu Photonics R5509 photomultiplier and a Q-switched Nd:YAG laser, which generated a second-harmonic (532 nm) pulse (20 Hz, 60 $\mu$J/pulse at the sample position). The gate time width was 2−100 $\mu$s. The samples (40 $\mu$M) were held in a quartz cuvette (optical path length 10 mm). The experiments were carried out in air at 22 °C. Quantum yield of $^1O_2$ ($\Phi_\Delta$) production by HSA−CF was determined using rose bengal as the standard compound.

**In Vitro Cytotoxicity Evaluation.** The LY80 tumor cell, a variant of the Yoshida sarcoma, was kindly gifted from Dr. Katsuyoshi Hori, Tohoku University. The cells were grown at 37 °C in DMEM supplemented with 10% fetal bovine serum (FBS) and penicillin (100 IU/$cm^3$) in 95% air−5% $CO_2$ humidified incubator. The cell solution (2.5 × $10^5$ cells/mL, 0.16 mL) was mixed with PBS (0.04 mL) or PBS solution of HSA−CF (100 $\mu$M, 0.04 mL) in a Corning Costar 3596 cell culture plate (96 well) and incubated in the dark. Then the plate was irradiated by visible light using a 500 W halogen lamp in conjunction with a HOYA HA30 heart absorption filter (330−700 nm). The power at the cell level was monitored using a Gentec Power Meter and adjusted to 20 mW $cm^{-2}$. The temperature was kept at 36 ± 1 °C during the irradiation. As a negative control, we examined another PBS group in the same culture plate without light irradiation. After 2 h, the cell numbers were counted using microscopy under tripan blue staining.

## RESULTS AND DISCUSSION

**Structure of HSA−Fullerene Complexes.** The HSA−fullerene complexes were prepared essentially as described previously for HSA−hemin complexes (*21*). A phosphate buffered (PB) solution (pH 7.0, 50 mM) of HSA was mixed with PB solution of CF (CF/HSA molar ratio of 1:1) and incubated for 12 h. The complex was then concentrated to the initial volume using a centrifuge filter (Figure 1 inset photograph). The filtrate was colorless during the centrifugation. The gel permeation chromatogram (Superdex 75 g) of the orange-colored protein exhibited only a single elution peak. These results indicate that CF is efficiently incorporated into HSA. For comparison, hydrophobic fullerene, 2-[4-(2-hydroxyethoxy)-phenyl]-1,3-dioxolo-4a,5a-[60]fullerene (HF), was also complexed with HSA to give HSA−HF. The obtained HSA−fullerene solutions can be concentrated up to 3.75 mM (25 g $dL^{-1}$); they were stable for a year without precipitation.

The UV−vis absorption spectroscopic features of the HSA−CF solution are the sum of those from the individual HSA and CF (Figure 1), which indicates that CF is monomolecularly

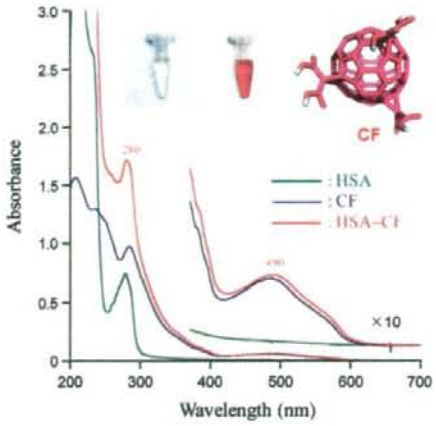


**Figure 1.** UV−vis absorption spectrum of HSA−CF complex, CF and HSA (20 $\mu$M) in PB solution (pH 7.0, 50 mM) at 22 °C. Inset photographs are 5 g dL$^{-1}$ HSA (left) and HSA−CF (right) solutions.

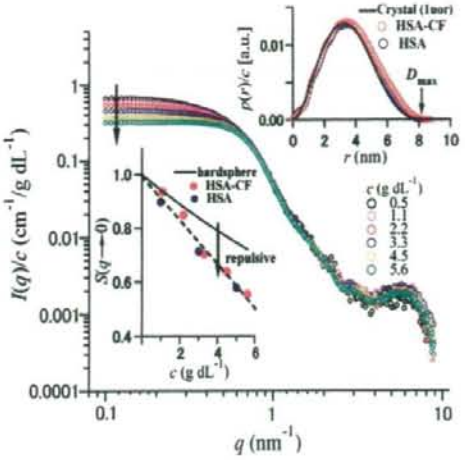


**Figure 2.** Normalized SAXS intensities [$I(q)/c$] of HSA−CF complex in 150 mM PBS solutions ($c$ = 0.5−5.6 g dL$^{-1}$). The upper and lower insets show pair-distance distribution functions [$p(r)$] and extrapolated structure factors [$S(q\to 0)$] of HSA−CF and HSA, respectively.

incorporated into HSA and no specific interaction between the two molecules at the ground state. In contrast, the absorption spectrum of the brown-colored HSA−HF solution did not coincide with the superposition of the HSA and HF spectra (Figure S1). The increased absorbance at 380−550 nm suggests the formation of HF clusters in the protein (*11, 16*).

The HSA−CF complex was sufficiently stable to apply the HPLC measurement. In the elution profile, a single peak appeared at a retention time of 7.64 min, which was slightly earlier than that of HSA itself (7.75 min) (Figure S2). The ratio of the peak intensity monitored at 280 nm (based on HSA) and at 490 nm (based on CF) ($I_{280}/I_{490}$ = 30) was exactly the same as the absorbance ratio at 280 and 490 nm in the UV−vis absorption spectrum ($A_{280}/A_{490}$) of HSA−CF, which implies that all CF molecules were eluted within the HSA fraction.

The ESI-TOF mass spectroscopy of HSA−CF showed a distinct ion peak at 67 587 Da, which corresponds to the mass of the equivalent complex of HSA−CF. On the other hand, two separated peaks were observed in the HSA−HF spectrum at 66 585 (free HSA) and 68 296 Da, that reveals 1:2 stoichiometry for HSA/HF and the formation of HF clusters in the protein. The CD spectral patterns and intensities of HSA−CF and HSA−HF were identical to those of HSA (Figure S3). We inferred that fullerene binding did not change the highly ordered structure of the host HSA.

The incorporation of negatively charged CF having hexacarboxyl groups might influence the surface charge distribution of albumin. However, isoelectric focusing of HSA−CF indicated the same isoelectric point ($p$I) with HSA. This contrasts sharply to the fact that fatty acid binding induced the reduction of the $p$I value because of partial neutralization of the molecular charge (*22*). We then used small-angle X-ray scattering (SAXS) to evaluate the globular particle structure and protein−protein interactions of HSA−CF (Figure 2) (*23*). The pair-distance distribution functions [$p(r)$] of HSA−CF and HSA were almost identical to the curve calculated from crystallographic data of HSA (1uor) (Figure 2 upper inset). It demonstrates that the maximum diameter ($D_{max}$: *ca.* 8 nm) and three-dimensional particle shape of HSA were unaltered by complexation of CF. The normalized SAXS intensities [$I(q)/c$] of HSA−CF at the low $q$ range [$I(q\to 0)/c$] monotonously decreases with increasing protein concentration. In the PBS solution, the long-range electrostatic repulsion between HSA−CFs is efficiently screened, so that the suppressed forward intensity could be mainly due to excluded volume effect. However, the extrapolated structure factors [$S(q\to 0)$] of HSA−CF and HSA, which reflect the net repulsive forces between the protein molecules, were systematically lower than that predicted for hardsphere with an identical volume fraction (Figure 2 lower inset). The negative deviations are attributed to the electrostatic repulsion between the proteins. It is remarkable that the plots of $S(q\to 0)$ for HSA−CF and HSA perfectly lie on the same line, suggesting that HSA preserves its surface net charges upon the CF binding. On the basis of these results, we conclude that (i) CF is accommodated into the deep hydrophobic cavity of HSA with internal charge neutralization, and (ii) it does not induce marked changes in the globular particle size and surface charge distribution of HSA.

**Photoexcited Triplet State of HSA−CF Complex and $^1O_2$ Formation.** Photoexcitation of the fullerenes generates the singlet state, which undergoes intersystem crossing to the triplet state in high yield (*10, 11*). Laser flash photolysis (SHG of Nd:YAG, 532 nm, 6 ns) of the HSA−CF solution under an $N_2$ atmosphere gave a triplet−triplet (T-T) absorption spectrum of the $^3$CF* chromophore ($\lambda_{max}$ = 740 nm) (Figure 3) (*11, 13, 24*). The time course of the absorbance decay was composed of a single exponential kinetics with a lifetime ($\tau_T$) of 46 $\mu$s (Figure 3 inset). The peaks of maximum absorption and $\tau_T$ value resembled those of the aqueous CF solution ($\tau_T$: 43 $\mu$s). These observations again support that CF is held monomolecularly within the HSA interior.

Although HF in DMSO exhibited clear triplet absorption ($\tau_T$: 31 $\mu$s), HSA−HF showed no signals in this wavelength range (Figure S4). The extremely short triplet lifetime of HSA−HF is probably attributed to T-T annihilation of the HF aggregates in the protein (*11*). If this is the case, the lifetime should become longer when the laser pulse energy is decreased. However, the decay was too fast to analyze precisely even under the weak laser flash photolysis.

In the presence of $O_2$, the triplet lifetime of HSA−CF significantly decreased. Energy transfer occurred from HSA−$^3$CF* to the $O_2$ molecule to generate active $^1O_2$. The Stern-Volmer plot clearly depicts a linear correlation for $O_2$ concentrations of 0−1.0 mM, giving the Stern-Volmer constant ($K_{SV}$) and quenching rate constant [$k_q(O_2)$] (Figure 4) [Note: $\tau_T^0/\tau_T = K_{SV}[O_2]$ ($\tau_T^0$ and $\tau_T$ represent triplet lifetimes in the absence and presence of $O_2$)].The $k_q(O_2)$ of HSA−CF was 2.2 × 10$^8$ M$^{-1}$ s$^{-1}$, which is one-seventh that of the monomeric

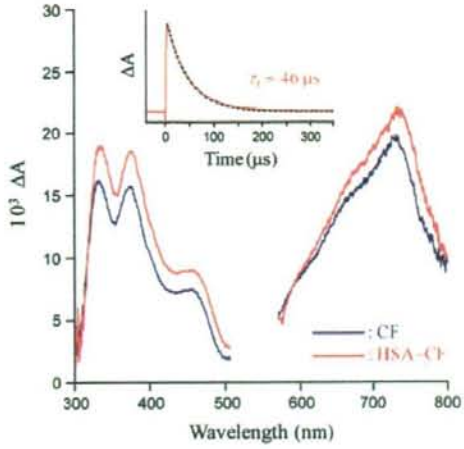


**Figure 3.** Triplet−triplet absorption spectra of HSA−CF complex and CF in PB solution (pH 7.0, 50 mM) under $N_2$ atmosphere at 22 °C; Ex. at 532 nm. The inset shows absorption decay of HSA−$^3$CF* complex at 734 nm, which was fitted by single exponential relaxation curve (black dotted line).

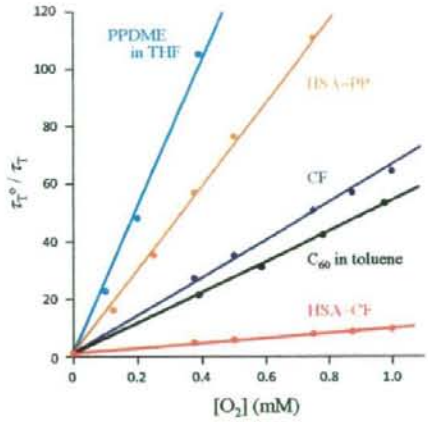


**Figure 4.** Stern-Volmer plots of triplet state quenching of HSA−CF complex and other compounds by $O_2$ at 22 °C. The HSA−CF, HSA−PP, and CF were in PB solution (pH 7.0, 50 mM).

**Table 1. Quenching Rate Constants of the Photoinduced Excited Triplet States of HSA−CF Complex and Other Compounds by $O_2$ at 22 °C**

| compound | solvent | $k_q(O_2)$ ($M^{-1}$ $s^{-1}$) |
|---|---|---|
| HSA−CF | PB (pH 7.0, 50 mM) | $2.2 \times 10^8$ |
| CF | PB (pH 7.0, 50 mM) | $1.6 \times 10^9$ |
| HSA−PP | PB (pH 7.0, 50 mM) | $1.3 \times 10^8$ |
| PPDME | THF | $1.6 \times 10^9$ |
| $C_{60}$ | toluene | $1.6 \times 10^9$ |
| | | $1.9 \times 10^{9a}$ |

[a] ref 10.

CF solution ($1.6 \times 10^9$ $M^{-1}$ $s^{-1}$) (Table 1). The HSA−PP complex in PB also showed smaller $k_q(O_2)$ ($1.3 \times 10^8$ $M^{-1}$ $s^{-1}$) compared to that of the protoporphyrin IX dimethylester (PPDME) in THF (*25*). The slow $k_q(O_2)$ values of the protein systems suggest that the quenching reaction is almost diffusion controlled. The intensity of the visible band of HSA−CF ($\lambda_{max}$ = 490 nm) did not changed after $10^3$ laser flash photolysis ($\lambda_{ex}$ = 532 nm, 0.5 W) in air, indicating no photodegradation of the CF chromophore. In contrast, the Soret band of HSA−PP was

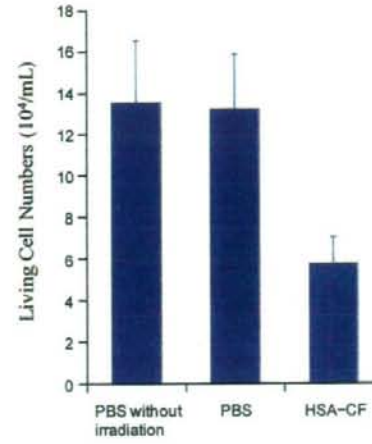


**Figure 5.** Living cell numbers of LY80 with HSA−CF and PBS after visible light irradiation (20 mW $cm^{-2}$, 2 h, 36 ± 1 °C). Each value represents the mean ± SD ($n$ = 4).

≈6% photobleached after the identical flash irradiations. It can be concluded that the light resistance of CF is significantly higher than that of PP, which is an active photosensitizer in ALA-PDT.

We observed the near-infrared luminescence of the produced $^1O_2$ ($\lambda_{max}$ 1270 nm) and evaluated the quantum yield of $^1O_2$ production ($\Phi_\Delta$) for HSA−CF from the value of emission intensity at 1270 nm ($I$) using rose bengal as a standard (*26*). The $\Phi_\Delta$ value of HSA−CF (0.46) was in the same range as those of monomeric CF (0.48), methylene blue (0.52), PPDME in benzene (0.59) (*26*), and substituted fullerenes in organic solvent (*27, 28*), but somewhat lower than those of rose bengal (0.75), hematoporphyrin in methanol (0.74) (*29*), and $C_{60}$ (0.96) in benzene (*10*). It is known that the substitution of the pristine $C_{60}$ causes a perturbation of the electronic structure of the fullerene core, and thereby results in a decrease in the quantum yield for the $^1O_2$ formation (*27, 28*).

**Cytotoxicity of HSA−CF Complex.** Finally, we measured the cytotoxicity and photodynamic activity of the HSA−CF complex to the LY80 tumor cells in vitro. The cell cultures were first incubated for 24 h in the dark with HSA−CF (20 μM) at 37 °C under 5% $CO_2$. The cell numbers after the incubation were identical to that of control group with the PBS solution, indicating that the HSA−CF complex does not have dark cytotoxicity. The cell culture plates were then exposed to visible light of 350−600 nm (20 mW $cm^{-2}$) for 2 h at 36 ± 1 °C. Some of the cells mixed with HSA−CF showed abnormal shape after the light irradiation, whereas the PBS group did not show any morphological changes of the cells. The living cell numbers of the PBS groups with and without light irradiation were almost the same (Figure 5), which means that the light exposure did not affect the LY80 tumor cells in this experimental condition. On the other hand, the living cell numbers of the HSA−CF group were markedly lower than that of the PBS group; 57% cell death occurred by visible light irradiation. This result clearly implies that the HSA−CF complex acts as a photosensitizer for PDT.

## CONCLUSIONS

The HSA−CF complex having identical molecular shape and surface charge distribution with HSA is easily excited by visible light and shows a high charge transfer rate constant for molecular $O_2$. The efficiency of the $^1O_2$ production of this artificial protein is in the same range as well-known dye

sensitizers, such as methylene blue and PPDME. In general, water-soluble drugs administrated into our bloodstream are quickly eliminated from the body. On the contrary, the HSA hybrid can remain in the circulatory system and/or tissues with a long persistence; therefore, the $^1O_2$ generation by albumin-based photosensitizer might be of clinical importance for photodynamic cancer therapy. The HSA−CF complex does not show dark cytotoxicity, but engenders cell death efficiently under visible light irradiation. Recombinant HSA is currently manufactured on an industrial scale using yeast species *Pichia pastoris* (*30*), which allows the use of the HSA−fullerene complex in practical applications.

## ACKNOWLEDGMENT

This work was supported by PRESTO, JST, and Grant-in-Aid for Scientific Research from JSPS (No. 20350058), and Health Science Research Grants from MHLW, Japan. The authors acknowledge Dr. Akifumi Kamiya (Hamamatsu Photonics KK) for near-infrared photocounting measurements. X.Q. thanks a JSPS Postdoctoral Fellowship for Foreign Researchers.

**Supporting Information Available:** Figures S1−S4. This material is available free of charge via the Internet at http://pubs.acs.org.

## LITERATURE CITED

(1) Dougherty, T. J., Gomer, C. J., Henderson, B. W., Jori, G., Kessel, D., Korbelik, M., Moan, J., and Peng, Q. (1998) Photodynamic therapy. *J. Natl. Cancer Inst. 90*, 889–905.

(2) Sharman, W. M., Allen, C. M., and Lier, J. E. (1999) Photodynamic therapeutics: basic principles and clinical applications. *Drug Discovery Today 4*, 507–517.

(3) Sternberg, E. D., Dolphin, D., and Bruckner, C. (1998) Porphyrin-based photosensitizers for use in photodynamic therapy. *Tetrahedron 54*, 4151–4202.

(4) Dougherty, T. J. (1987) Studies on the structure of porphyrins contained in Photofrin-II. *Photochem. Photobiol. 46*, 569–573.

(5) Aveline, B., Hasen, T., and Redmond, R. W. (1994) Photophysical and photosensitizing properties of benzoporphyrin derivative monoacid ring A (BPD-MA). *Photochem. Photobiol. 59*, 328–335.

(6) Kato, H., Furukawa, K., Sato, M., Okunaka, T., Kusunoki, Y., Kawahara, M., Fukuoka, M., Miyazawa, T., Yana, T., Matsui, K., Shiraishi, T., and Horinouchi, H. (2003) Phase II clinical study of photodynamic therapy using mono-L-aspartyl chlorine e6 and diode laser for early superficial squamous cell carcinoma of the lung. *Lung Cancer 42*, 103–111.

(7) Kennedy, J. C., Pottier, R. H., and Pross, D. C. (1990) Photodynamic therapy with endogeneous protoporphyrin IX: basic principles and present clinical experience. *J. Photochem. Photobiol. B 6*, 143–148.

(8) Lopez, R. F. V., Lange, N., Guy, R., and Bentley, M. V. L. B. (2004) Photodynamic therapy of skin cancer: controlled drug delivery of 5-ALA and its esters. *Drug Delivery Rev. 56*, 77–94.

(9) Peng, Q., Warloe, T., Berg, K., Moan, J., Kongshaug, M., Giercksky, K. E., and Nesland, J. M. (1997) 5-Aminolevulic acid-based photodynamic therapy -clinical research and future challenges. *Cancer 79*, 2282–2308.

(10) Arbogast, J. W., Darmanyan, A. P., Foote, C. S., Rubin, Y., Diederich, F. N., Alvarez, M. M., Anz, S. J., and Whetten, R. L. (1991) Photophysical properties of $C_{60}$. *J. Phys. Chem. 95*, 11–12.

(11) Guldi, D. M., and Prato, M. (2000) Excited-state properties of $C_{60}$ fullerene derivatives. *Acc. Chem. Res. 33*, 695–703.

(12) Nakamura, E., and Isobe, H. (2003) Functionalized fullerene in water. The first 10 years of their chemistry, biology, and nanooscience. *Acc. Chem. Res. 36*, 807–815.

(13) Andersson, T., Nilsson, K., Sundahl, M., Westman, G., and Wennerström, O. (1992) $C_{60}$ embedded in γ-cyclodextrin: a water-soluble fullerene. *Chem. Commun.* 604–606.

(14) Yoshida, Z., Takekuma, H., Takekuma, S., and Matsubara, Y. (1994) Molecular recognition of $C_{60}$ with γ-cyclodextrin. *Angew. Chem., Int. Ed. 33*, 1597–1599.

(15) Islam, S. D.-M., Fjitsuka, M., Ito, O., Ikeda, A., Hatano, T., and Shinkai, S. (2000) Photoexcited state properties of $C_{60}$ encapsulated in a water-soluble calixarene. *Chem. Lett.* 78–79.

(16) Buvári-Barcza, A., Rohonczy, J., Rozlosnik, N., Gilányi, T., Szabo, B., Lovas, G., Braun, T., Samu, J., and Barcza, L. J. (2001) Aqueous solubilization of [60]fullerene via inclusion complex formation and the hydration of $C_{60}$. *J. Chem. Soc., Perkin Trans. 2*, 191–196.

(17) Kragh-Hansen, U. (1981) Molecular aspects of ligand binding to serum albumin. *Pharmacol. Rev. 33*, 17–53.

(18) Peters, T. (1996) *All about albumin: biochemistry, genetics and medical applications*, Academic Press Inc., San Diego.

(19) Dugan, L. L., Turetsky, D. M., Du, C., Lobner, D., Wheeler, M., Almli, C. R., Shen, C. K.-F., Luh, T.-Y., Choi, D. W., and Lin, T.-S. (1997) Carboxyfullerenes as neuroprotective agents. *Proc. Natl. Acad. Sci. U.S.A. 94*, 9434–9439.

(20) Benyamini, H., Shulman-Peleg, A., Wolfson, H. J., Belgorodsky, B., Fadeev, L., and Gozin, M. (2006) Formation and characterization of stable human serum albumin-tris-malonic acid [$C_{60}$]fullerene complex. *Bioconjugate Chem. 17*, 378–386.

(21) (a) Komatsu, T., Ohmichi, N., Nakagawa, A., Zunszain, P. A., Curry, S., and Tsuchida, E. (2005) $O_2$ and CO binding properties of artificial hemoproteins formed by complexing iron protoporphyrin IX with human serum albumin. *J. Am. Chem. Soc. 127*, 15933–15942. (b) Komatsu, T., Wang, R.-M., Zunszain, P. A., Curry, S., and Tsuchida, E. (2006) Photosensitized reduction of water to hydrogen using human serum albumin complexed with zinc-protoporphyrin IX. *J. Am. Chem. Soc. 128*, 16297–16301. (c) Komatsu, T., Matsukawa, Y., and Tsuchida, E. (2002) Effect of heme structure on $O_2$-binding properties of human serum albumin-heme hybrids: intramolecular histidine coordination provides a stable $O_2$-adduct complex. *Bioconjugate Chem. 13*, 397–402.

(22) Evenson, M. A., and Deutsch, H. F. (1978) Influence of fatty acids on the isoelectric point properties of human serum albumin. *Clin. Chim. Acta 89*, 341–354.

(23) Fritz, G., Bergmann, A., and Glatter, O. (2000) Evaluation of small-angle scattering data of charged particles using the generalized indirect Fourier transformation technique. *J. Chem. Phys. 113*, 9733–9740.

(24) Anderson, J. L., An, Y.-Z., Rubin, Y., and Foote, C. S. (1994) Photophysical characterization and singlet oxygen yield of a dihydrofullerene. *J. Am. Chem. Soc. 116*, 9763–9764.

(25) Kubát, P., Zelinger, Z., and Jirsa, M. (1997) The effect of the irradiation wavelength on the processes sensitized by protoporphyrin IX dimethyl ester. *Radiat. Res. 148*, 382–385.

(26) Wilkinson, F., Helman, W. P., and Rossa, A. B. (1993) Quantum yields for the photosensitized formation of the lowest electronically excited singlet-state of molecular-oxygen in solution. *J. Phys. Chem. Ref. Data 22*, 113–262.

(27) Hamano, T., Okuda, K., Mashino, T., Hirobe, M., Arakane, K., Ryu, A., Mashiko, S., and Nagano, T. (1997) Singlet oxygen production from fullerene derivatives: effect of sequential functionalization of the fullerene core. *Chem. Commun.* 21–22.

(28) Prat, F., Stackow, R., Bernstein, R., Qian, W., Rubin, Y., and Foote, C. S. (1999) Triplet-state properties and singlet oxygen generation in a homologous series of functionalized fullerene derivatives. *J. Phys. Chem. A 103*, 7230–7235.

(29) Tanielian, C., Wolff, C., and Esch, M. (1996) Singlet oxygen production in water: aggregation and charge-transfer effects. *J. Phys. Chem. 100*, 6555–6560.

(30) Kobayashi, K. (2006) Summary of recombinant human serum albumin development. *Biologicals 34*, 55–59.

BC800207J

MARCH 2008
Volume 19, Number 3



Bioconjugate Chemistry

# COMMUNICATIONS

## $O_2$ Binding to Human Serum Albumin Incorporating Iron Porphyrin with a Covalently Linked Methyl-L-Histidine Isomer

Akito Nakagawa,[†] Teruyuki Komatsu,*[,†,‡] Makoto Iizuka,[†] and Eishun Tsuchida*[,†]

Research Institute for Science and Engineering, Waseda University, 3-4-1 Okubo, Shinjuku-ku, Tokyo 169-8555, Japan, and PRESTO, Japan Science and Technology Agency (JST), 4-1-8 Honcho, Kawaguchi-shi, Saitama 332-0012, Japan. Received October 30, 2007; Revised Manuscript Received December 1, 2007

We describe the significant difference in the $O_2$ binding affinities of human serum albumin (HSA) incorporating 5,10,15,20-tetrakis{α,α,α,α-*o*-(1′-methylcyclohexanamido)phenyl}porphinatoiron(II) with a covalently linked 1-methyl-L-histidine or 3-methyl-L-histidine [HSA-FeP(1-MHis), HSA-FeP(3-MHis)]. The HSA-FeP(3-MHis) showed an extraordinarily high $O_2$ binding affinity ($P_{1/2}$ = 0.2 Torr, 25 °C, pH 7.4), which is close to those of relaxed-state hemoglobin and myoglobin. However, replacement of the 3-methyl-L-histidine moiety in FeP(3-MHis) by 1-methyl-L-histidine caused a 35-fold reduction in $O_2$ affinity; the $P_{1/2}$ value of HSA-FeP(1-MHis) (22 Torr, 37 °C, pH 7.4) is almost identical to that of human red blood cells. Results of kinetic studies indicate that the low $O_2$ binding affinity of FeP(1-MHis) is predominantly manifested in the high $O_2$ dissociation rate constant. In a toluene solution, an identical relationship in the $O_2$ binding property was similarly observed for FeP(1-MHis) and FeP(3-MHis). The axial Fe-N(1-MHis) coordination might be restrained by steric interaction between the 4-methylene group of the histidine and the porphyrin plane.

Numerous synthetic model hemes have been prepared to mimic the $O_2$ binding capability of hemoglobin (Hb) and myoglobin (Mb) over the past few decades (*1–3*). In these highly modified iron(II) porphyrins, axial coordination of the nitrogenous base plays a crucial role in regulating $O_2$ binding affinity. Collman and co-workers demonstrated that picket-fence porphyrin[1] ligating a 1,2-dimethylimidazole (1,2-DMIm) showed a 70-fold lower $O_2$ binding affinity [$P_{1/2}$ ($O_2$ partial pressure at which 50% of porphyrin was dioxygenated) = 38 Torr, 25 °C] than that of the complex with 1-methylimidazole (1-MIm) (*4, 5*). This reduction was ascribed to the steric interaction between the 2-methyl group of the imidazole and the porphyrin plane. Furthermore, they showed that the replacement of imidazole by pyridine in the tailed picket-fence porphyrin lowered the $O_2$-binding affinity by a factor of 40 (*6*). The weaker π-basicity of pyridine and the increased steric repulsion of the six-atom pyridine ring compared to that of the five-atom imidazole reduced the $O_2$ binding of the iron(II) porphyrins (*7–10*). We previously reported that 2-[{8-*N*-(methylimidazolyl)octanoyloxy}methyl]-5,10,15,20-tetrakis{α,α,α,α-*o*-(1′-methylcyclohexanamido)phenyl}porphinatoiron(II) [FeP(2-MIm)] formed a stable $O_2$ adduct in toluene solution, and human serum albumin (HSA) incorporating FeP(2-MIm) [HSA-FeP(2-MIm)]

* Corresponding author. Tel: +81-3-5286-3120. Fax: +81-3-3205-4740. E-mail: eishun@waseda.jp (E.T.). E-mail: teruyuki@waseda.jp (T.K.).
[†] Waseda University.
[‡] Japan Science and Technology Agency (JST).
[1] Picket-fence porphyrin: 5,10,15,20-tetrakis{(α,α,α,α-o-pivalamido)-phenyl}porphinatoiron.

10.1021/bc700400n CCC: $40.75 
Published on Web 01/19/2008

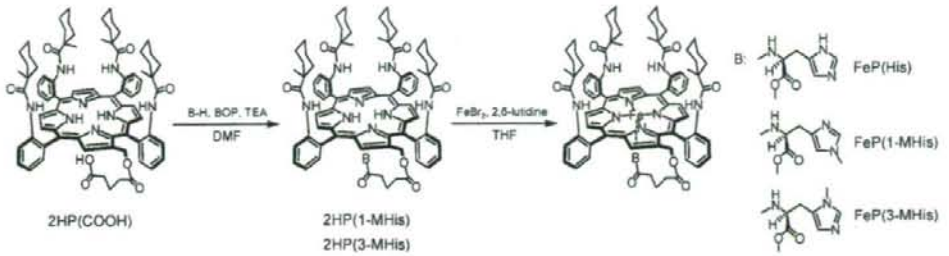


**Figure 1.** Synthetic scheme of iron(II) porphyrin bearing a covalently linked histidine derivative as an axial base at the $\beta$-pyrrolic position.

can bind $O_2$ not only in aqueous media (pH 7.4) but also in the blood stream as an artificial red blood cell (RBC) substitute (*11, 12*). For practical biomedical applications of the synthetic iron(II) porphyrin as an $O_2$ carrier, two physiological requirements exist. First, $O_2$ binding affinity should be close to that of human RBC ($P_{1/2}$ = 27 Torr, 37 °C). Second, it is favorable to use natural histidine as an axial base because some imidazole and pyridine derivatives show toxicity to respiratory organs and the central nervous system (*13*). Nevertheless, few studies have addressed $O_2$ binding of the synthetic model heme having a histidyl group (*14–16*). We have demonstrated the $O_2$ binding equilibrium and kinetics of 5,10,15,20-tetrakis{α,α,α,α-*o*-(1′-methylcyclohexanamido)phenyl}porphinatoiron(II) with an ω-histidylalkyl chain [FeP(His)[2]] (*17*). A new class of biocompatible $O_2$ carriers would be realized if we can regulate $O_2$ binding affinity by changing the steric and electronic natures of the attached histidine. We now report a significant difference in the $O_2$ binding properties of HSA hybrid with synthetic iron(II) porphyrin bearing a covalently linked 1-methyl-L-histidine or 3-methyl-L-histidine [HSA-FeP(1-MHis) and HSA-FeP(3-MHis)] (Figure 1) under physiological conditions (pH 7.4, 37 °C).

The 1-methyl-L-histidine methylester or 3-methyl-L-histidine methylester was introduced into the carboxyl group of the parent free-base porphyrin, 2-{(4-carboxybutanoyloxy)methyl}-5,10,15,20-tetrakis{α,α,α,α-*o*-(1′-methylcyclohexanamido)phenyl}porphin [2HP(COOH)] (*11*), via an amide linkage, yielding histidine-terminated porphyrins (>60% yield) (Figure 1). The cyclohexanoyl substituents stabilized the $O_2$ adduct complex rather than the pivaloy group (*11*). The central iron was inserted as iron(II) using $FeBr_2$ and 2,6-lutidine in anhydrous THF. The analytical data of all compounds were satisfactorily obtained (see Supporting Information).

Both FeP(1-MHis) and FeP(3-MHis) are readily incorporated into HSA (Mw: 66.5 kDa), producing stable artificial hemoproteins: HSA-FeP(1-MHis) and HSA-FeP(3-MHis) [in phosphate-buffered saline (PBS) solution at pH 7.4, [porphyrin]/[HSA] = 4 (mol/mol)]. The UV–vis absorption spectra of the aqueous HSA-FeP(1-MHis) and HSA-FeP(3-MHis) solutions under an $N_2$ atmosphere showed a similar feature of HSA-FeP(2-MIm) and HSA-FeP(His) (Figure 2) (Table S1) (*11, 17*). The spectral shapes resembled those of the five-N-coordinate high-spin ferrous complex of picket-fence porphyrin and other tetraphenylporphyrin derivatives (*5*). These results indicated that FeP(1-MHis) and FeP(3-MHis) formed a five-N-coordinate high-spin complex with an intramolecularly coordinated methyl-

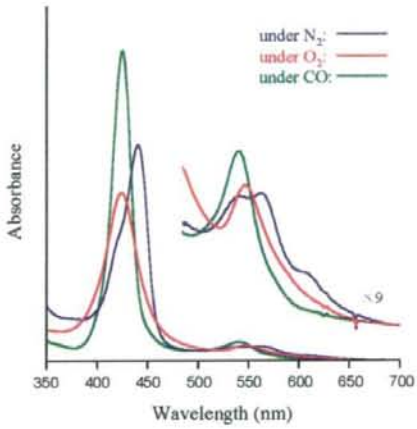


**Figure 2.** UV–vis absorption spectral changes of HSA-FeP(1-MHis) in PBS solution at 25 °C.

L-histidine moiety in the protein matrix. Upon bubbling of $O_2$ gas into the solution, the absorption pattern changed immediately to that of the $O_2$ adduct complex. The dioxygenations of these artificial hemoproteins have been observed reversibly under physiological conditions (pH 7.4, 37 °C). After passing the CO gas, the absorption maxima shifted to that of the carbonyl complex.

The $O_2$ binding affinities [$K = (P_{1/2})^{-1}$] of HSA-FeP(1-MHis) and HSA-FeP(3-MHis) were determined by the absorption spectral changes at various $O_2$ concentrations (eq 1).

$$\mathrm{FeP(B)} + \mathrm{O_2} \underset{k_{off}}{\overset{k_{on}}{\rightleftharpoons}} \mathrm{FeP(B)\text{-}O_2} \qquad [K = (P_{1/2})^{-1}] \tag{1}$$

The HSA-FeP(3-MHis) showed an extraordinarily high $O_2$ binding affinity ($P_{1/2}$ = 0.2 Torr, 25 °C), which is 5-fold greater than that of HSA-FeP(His), which was close to the values of the relaxed-state Hb(α) and Mb (Table 1) (*18–20*). However, replacement of the 3-methyl-L-histidine moiety in FeP(3-MHis) by the 1-methyl-L-histidine isomer [FeP(1-MHis)] caused a 35-fold reduction of $O_2$ binding affinity ($P_{1/2}$ = 7 Torr, 25 °C); the $P_{1/2}$ value of 22 Torr at 37 °C was almost identical to that of human RBC (27 Torr) (*21*).

Laser flash photolysis experiments gave the association and dissociation rate constants for $O_2$ ($k_{on}$, $k_{off}$) (*5, 11*). The time course of the absorption change accompanying the $O_2$ recombinations to HSA-FeP(1-MHis) and HSA-FeP(3-MHis) after the laser pulse irradiation comprised two phases of first-order kinetics (Figure S1a). The decay was fitted by a double exponential profile, which provided the fast and slow association rate constants of $O_2$ ($k_{on}$ and $k'_{on}$) (Table 1). This behavior was similarly observed in HSA-

[2] Abbreviations: FeP(His), 2-{(4-methoxycarbonyl-histidinamidobutanoyloxy)methyl}-5,10,15,20-tetrakis{α,α,α,α-o-(1′-methylcyclohexanamido)phenyl}porphinatoiron; FeP(1-MHis), 2-[{4-methoxycarbonyl(1-methyl)histidinamidobutanoyloxy}methyl]-5,10,15,20-tetrakis{α,α,α,α-o-(1′-methylcyclohexanamido)phenyl}porphinatoiron; FeP(3-MHis), 2-[{4-methoxycarbonyl(3-methyl)histidinamidobutanoyloxy}methyl]-5,10,15,20-tetrakis{α,α,α,α-o-(1′-methylcyclohexanamido)phenyl}porphinatoiron.

**Table 1. $O_2$ Binding Parameters of Human Serum Albumin Hybrid with Iron(II) Porphyrin Bearing a Methyl-L-Histidine Isomer in PBS Solution (pH 7.4) at 25 °C**

| HSA-iron(II) porphyrin | $k_{on}$ ($M^{-1}$ $s^{-1}$) | $k'_{on}$ ($M^{-1}$ $s^{-1}$) | $k_{off}$ ($s^{-1}$) | $k'_{off}$ ($s^{-1}$) | $P_{1/2}$[a] (Torr) |
|---|---|---|---|---|---|
| HSA-FeP(1-MHis) | $5.4 \times 10^7$ | $8.1 \times 10^6$ | 620 | 93 | 7 (22) |
| HSA-FeP(3-MHis) | $5.4 \times 10^7$ | $6.8 \times 10^6$ | 20 | 2.4 | 0.2 (1) |
| HSA-FeP(His)[b] | $5.4 \times 10^7$ | $8.8 \times 10^6$ | 89 | 14 | 1 (3) |
| Hb(α) (R-state)[c] | $3.3 \times 10^7$[d] | | 13[e] | | 0.24 |
| Mb[f,g] | $1.4 \times 10^7$ | | 12 | | 0.51 |
| RBC[h] | | | | | 8 (27) |

[a] At 37 °C in parenthesis. [b] Ref *11*. [c] Human Hb α-subunit. [d] In 0.1 M phosphate buffer (pH 7.0, 21.5 °C); ref *18*. [e] In 10 mM phosphate buffer (pH 7.0, 20 °C); ref *19*. [f] Sperm whale Mb. [g] In 0.1 M phosphate buffer (pH 7.0, 20 °C); ref *20*. [h] Human red blood cell suspension. In isotonic buffer (pH 7.4); ref *21*.

**Table 2. $O_2$ Binding Parameters of Iron(II) Porphyrin Bearing a Methyl-L-Histidine in Toluene Solution at 25 °C**

| iron(II) porphyrin | $k_{on}$ ($M^{-1}$ $s^{-1}$) | $k_{off}$ ($s^{-1}$) | $P_{1/2}$ (Torr) |
|---|---|---|---|
| FeP(1-MHis) | $9.8 \times 10^7$ | $3.5 \times 10^4$ | 27 |
| FeP(3-MHis) | $1.6 \times 10^8$ | $5.2 \times 10^2$ | 0.3 |
| FeP(His)[a] | $2.0 \times 10^8$ | $4.3 \times 10^3$ | 1.7 |

[a] In benzene solution, ref *17*.

FeP(His) and HSA-FeP(2-MIm) (*11*). It has been interpreted that the $O_2$ associations to the iron(II) porphyrins in HSA were affected by microenvironments around the accommodation site (steric hindrance of the amino acid residue and difference in polarity) (*22*). The kinetic data indicated that the low $O_2$ binding affinity of HSA-FeP(1-MHis) is predominantly manifested in the high $O_2$ dissociation rate constant (Table 1).

To evaluate the significant differences in FeP(1-MHis) and FeP(3-MHis), their $O_2$ binding parameters in toluene solution were determined. The UV–vis absorption spectra of ferrous FeP(1-MHis) ($\lambda_{max}$, 440, 542, 563 nm) and FeP(3-MHis) ($\lambda_{max}$, 440, 540, 565 nm) under an $N_2$ atmosphere showed the formation of a five-N-coordinate high spin complex. Dioxygenation was sufficiently stable and reversible at 25 °C depending on $O_2$ partial pressure. The recombination process of $O_2$ to the iron(II) porphyrins in toluene solution after laser flash photolysis was fitted by a single exponential (Figure S1b). FeP(3-MHis) exhibited a 6-fold higher $O_2$ binding affinity ($P_{1/2}$ = 0.3 Torr, 25 °C) compared to that of FeP(His) (Table 2) (*11*). Kinetically, this high $O_2$ binding affinity is attributable to the low $O_2$ dissociation rate. The high $\sigma$-basicity of 3-methyl-L-histidine (p*K*a, 6.48) in comparison to that of histidine (p*K*a, 6.00) (*23*) can serve to increase the electron density on the central metal, which would enhance $O_2$ uptake. FeP(1-MHis) showed a 90-fold lower $O_2$ affinity ($P_{1/2}$ = 27 Torr, 25 °C) relative to FeP(3-MHis), which is mainly caused by the high $k_{off}$ value, as observed in aqueous media. In general, the steric hindrance to the axial base coordination deforms the six-coordinate structure of the iron(II) porphyrin and increases the $O_2$ dissociation rate constant (*1, 2*). For example, the 1,2-DMIm complexes showed 11–58-fold higher $k_{off}$ values than the 1-MIm ligated complexes (*3, 5, 24*).

We simulated the geometry of histidine coordination in dioxygenated porphyrin.[3] The bond angle of N(por)−Fe−N(His) was 90° for FeP(His) and FeP(3-MHis), but it was markedly tilted in FeP(1-MHis) (a maximum of 98°) (Figure 3). On the basis of these results, it can be concluded that the axial coordination of 1-methyl-L-histidine to the central iron is

[3] The esff forcefield simulation was performed using an Insight II system (Molecular Simulations Inc.). The structure was generated by alternative minimizations and annealing dynamic calculations from 1,000 to 100 K.

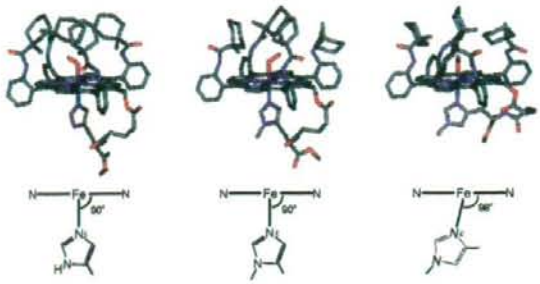


**Figure 3.** Simulated structures of the $O_2$ adduct complexes of FeP(His), FeP(3-MHis), and FeP(1-MHis). In FeP(His) and FeP(3-MHis), the bond angles of N(por)−Fe−N(His) were 90°, but 98° in FeP(1-MHis) because of the steric interaction between the 4-methylene group of histidine and the porphyrin plane. Molecular dynamics and minimization (force field: esff) were performed using an Insight II system. Hydrogens were omitted for clarification.

restrained by the steric interaction between the 4-methylene group of the histidine and the porphyrin plane, which significantly increased the dissociation rate of $O_2$.

In conclusion, a variation in the methyl-L-histidine isomer covalently linked at the porphyrin periphery changed the $O_2$ binding affinity of the iron(II) porphyrin by a factor of 90 in toluene. This difference is greater than the previous finding for a picket-fence porphyrin (2-MIm) complex-bound $O_2$ with a 70-fold lower affinity than that of the 1-MIm complex (*4*). The increased $k_{off}$ value of FeP(1-MHis) is caused by steric repulsion between the 4-methylene group of histidine and the porphyrin plane. In aqueous media, the $O_2$ binding ability of HSA incorporating the iron(II) porphyrin can also be modulated by structural isomerization of the axial methyl-L-histidine. HSA-FeP(1-MHis) with a $P_{1/2}$ value similar to that of human RBC under physiological conditions can become a promising $O_2$ carrier, which satisfies both the biocompatibility and clinical requirements for efficient $O_2$ delivery to the tissue cells.

## ACKNOWLEDGMENT

This work was partially supported by Grant-in-Aid for Young Scientists (B) (No. 18750156) from JSPS, PRESTO from JST, and Health Science Research Grants from MHLW, Japan.

**Supporting Information Available:** Experimental details, absorption maximum wavelengths of the iron(II) porphyrins, and absorption change accompanying $O_2$ rebinding to FeP(3-MHis) and HSA-FeP(3-MHis) after laser flash photolysis. This material is available free of charge via the Internet at http://pubs.acs.org.

## LITERATURE CITED

(1) Collman, J. P., Boulatov, R., Sunderland, C. J., and Fu, L. (2004) Functional analogues of cytochrome c oxidase, myoglobin, and hemoglobin. *Chem. Rev. 104*, 561–588.
(2) Collman, J. P., and Fu, L. (1999) Synthetic Models for Hemoglobin and Myoglobin. *Acc. Chem. Res. 32*, 455–463.
(3) Momenteau, M., and Reed, C. A. (1994) Synthetic heme-dioxygen complexes. *Chem. Rev. 94*, 659–698.
(4) Collman, J. P., Brauman, J. I., Doxsee, K. M., Halberd, T. M., and Suslick, K. S. (1978) Model compounds for the T state of hemoglobin. *Proc. Natl. Acad. Sci. U.S.A. 75*, 564–568.
(5) Collman, J. P., Brauman, J. I., Iverson, B. L., Sessler, J. L., Morris, R. M., and Gibson, Q. H. (1983) $O_2$ and CO binding to iron(II) porphyrins: A comparison of the "picket fence" and "pocket" porphyrins. *J. Am. Chem. Soc. 105*, 3052–3064.

(6) Collman, J. P., Brauman, J. I., Doxsee, K. M., Sessler, J., Morris, R. M., and Gibson, Q. H. (1983) Effect of axial base on dioxygen and carbon monoxide affinities of iron(II) porphyrins. Imidazole vs. pyridine. *Inorg. Chem. 22*, 1427–1432.

(7) Chang, C. K., and Traylor, T. G. (1975) Kinetics of oxygen and carbon monoxide binding to synthetic analogs of the myoglobin and hemoglobin active sites. *Proc. Nat. Acad. Sci. U.S.A. 72*, 1166–1170.

(8) Linard, J. E., Ellis, P. E., Jr., Budge, J. R., Jones, R. D., and Basolo, F. (1980) Oxygenation of iron(II) and cobalt(II) "capped" porphyrins. *J. Am. Chem. Soc. 102*, 1896–1904.

(9) Momenteau, M., Mispelter, J., Loock, B., and Lhoste, J.-M. (1985) Both-faces hindered porphyrins. Part 3. Synthesis and characterization of internally five-co-ordinated iron(II) basket handle porphyrins derived from 5,10,15,20-tetrakis(o-aminophenyl)porphyrin. *J. Chem. Soc., Perkin Trans.1* 221–231.

(10) Lavalette, D., Tetreau, C., Mispelter, J., Momenteau, M., and Lhoste, J.-M. (1984) Linear free-energy relationships in binding of oxygen and carbon monoxide with heme model compounds and heme proteins. *Eur. J. Biochem. 145*, 555–565.

(11) Komatsu, T., Matsukawa, Y., and Tsuchida, E. (2002) Effect of heme structure on $O_2$-binding properties of human serum albumin-heme hybrids: Intramolecular histidine coordination provides a stable $O_2$-adduct complex. *Bioconjugate Chem. 13*, 397–402.

(12) Komatsu, T., Huang, Y., Yamamoto, H., Horinouchi, H., Kobayashi, K., and Tsuchida, E. (2004) Exchange transfusion with synthetic oxygen-carrying plasma protein "albumin-heme" into an acute anemia rat model after seventy-percent hemodilution. *J. Biomed. Mater. Res. 71A*, 644–651.

(13) Sax, N. I., and Lewis, R. J. (1987) *Hazardous Chemicals Desk Reference*, Van Nostrand Reinhold Company, Inc., New York.

(14) Van der Heijden, A., Peter, H. G., and Van der Oord, A. H. A. (1971) Coupling of L-histidine methyl ester and L-histidine-containing peptide esters to ferric protoporphyrin IX chloride. *J. Chem. Soc. D* 369–370.

(15) Warme, P. K., and Hager, L. P. (1970) Heme sulfuric anhydrides. I. Synthesis and reactions of mesoheme sulfuric anhydride. *Biochemistry 9*, 1599–1606.

(16) Momenteau, M., Rougee, M., and Loock, B. (1976) Five-coordinate iron-porphyrin as a model for the active site of hemoproteins. Characterization and coordinating properties. *Eur. J. Biochem. 71*, 63–76.

(17) Komatsu, T., Matsukawa, Y., Miyatake, K., and Tsuchida, E. (2001) $O_2$-adduct complex of meso-tetrakis(α,α,α,α-o-pivalamidophenyl)porphinatoiron(II) with an intramolecularly coordinated proximal histidine. *Chem. Lett.* 668–669.

(18) Gibson, Q. H. (1970) The reaction of oxygen with hemoglobin and the kinetic basis of the effect of salt on binding of oxygen. *J. Biol. Chem. 245*, 3285–3288.

(19) Olson, J. S., Andersen, M. E., and Gibson, Q. H. (1971) The Dissociation of the first oxygen molecule from some mammalian oxyhemoglobins. *J. Biol. Chem. 246*, 5919–5923.

(20) Rohlfs, R., Mathews, A. J., Carver, T. E., Olson, J. S., Springer, B. A., Egeberg, K. D., and Sligar, S. G. (1990) The effects of amino acid substitution at position E7 (residue 64) on the kinetics of ligand binding to sperm whale myoglobin. *J. Biol. Chem. 265*, 3168–3176.

(21) Imai, K., Morimoto, H., Kotani, M., Watari, H., Hirata, W., and Kuroda, M. (1979) Studies on the function of abnormal hemoglobins I. An improved method for automatic measurement of the oxygen equilibrium curve of hemoglobin. *Biochim. Biophys. Acta 200*, 189–1967.

(22) Komatsu, T., Matsukawa, Y., and Tsuchida, E. (2000) Kinetics of CO and $O_2$ binding to human serum albumin-heme hybrid. *Bioconjugate Chem. 11*, 772–776.

(23) Lide, R. D., Eds. (2000) *CRC Handbook of Chemistry and Physics*, 81st ed., Section 7, CRC Press, Boca Raton, FL.

(24) Momenteau, M., Loock, B., Tetreau, C., Lavalette, D., Croisy, A., Schaeffer, C., Huel, and Lhoste, J.-M. (1987) Synthesis and characterization of a new series of iron(II) single-face hindered porphyrins. Influence of central steric hindrance upon carbon monoxide and oxygen binding. *J. Chem. Soc., Perkin Trans. 2* 249–257.

BC700400N

# Heme Pocket Architecture in Human Serum Albumin: Regulation of $O_2$ Binding Affinity of a Prosthetic Heme Group by Site-Directed Mutagenesis

*Teruyuki Komatsu,*[*1,2] *Akito Nakagawa,*[1] *Eishun Tsuchida*[*1]

**Summary:** We present the $O_2$ binding properties of recombinant human serum albumin (rHSA) mutants complexed with an iron(II) protoporphyrin IX as a prosthetic heme group. Iron(III) protoporphyrin IX (hemin) is bound within subdomain IB of HSA with weak axial coordination by Tyr-161. In order to confer $O_2$ binding capability to this naturally occurring hemoprotein: (i) a proximal histidine was introduced into position Ile-142; and (ii) the coordinated Tyr-161 was replaced with hydrophobic Leu using site-directed mutagenesis. It provided a recombinant HSA double-mutant [rHSA(I142H/Y161L) = rHSA(HL)]. The rHSA(HL)–heme formed a ferrous five-coordinate high-spin complex with axial ligation of His-142 under an Ar atmosphere. This artificial hemoprotein binds $O_2$ at room temperature. Laser flash photolysis experiments demonstrated that $O_2$ rebinidng to rHSA(HL)–heme displays monophasic kinetics, whereas the CO recombination process obeyed a double-exponential pattern. This might be attributable to the two different geometries of the axial imidazole coordination arising from the two orientations of the porphyrin plane in the heme pocket. The $O_2$ binding affinity of rHSA(HL)–heme was considerably lower than those of R-state hemoglobin (Hb) and myoglobin (Mb), principally because of the high $O_2$ dissociation rate constant. The third mutations have been introduced into the distal side of the heme (at position Leu-185 or Arg-186) to increase the $O_2$ binidng affinity. The rHSA(HL/L185N)–heme showed high $O_2$ binding affinity ($P^{O_2}_{1/2}$: 1 Torr), which is 18-fold greater than that of the original double mutant rHSA(HL)–heme and which is rather close to those of Hb (R-state) and Mb. Furthermore, replacement of polar Arg-186 with Leu or Phe adjusted the $O_2$ binding affinity ($P^{O_2}_{1/2}$) to 10 Torr, which is almost equivalent to value for human red blood cells.

**Keywords:** biomimetics; heme; human seruma albumin; $O_2$ binidng; proteins

## Introduction

Human serum albumin (HSA), the most abundant plasma protein (4–5 g/dl) in our circulatory system, is characterized by its remarkable ability to bind widely various endogenous and exogenous compounds[1] such as fatty acids, bilirubin, bile acids, thyroxine,[2,3] and a wide range of drugs.[4] Hemin [iron(III) protoporphyrin IX] released from methemoglobin is also captured by HSA with a high binding constant ($K \approx 10^8$ $M^{-1}$).[5] This strong affinity of HSA for hemin has stimulated efforts to develop albumin as an artificial hemoprotein which can mimic the $O_2$ binding ability of hemoglobin (Hb) and myoglobin (Mb).[6,7] HSA consists of a helical monomer of 66.5 kDa containing three homologous domains (I–III), each of which comprises of A and B subdomains.[8] Crystallographic

[1] Research Institute for Science and Engineering, Waseda University, 3-4-1 Okubo, Shinjuku-ku, Tokyo 169-8555, Japan
Fax: (+81) 3-3205-4740;
E-mail: teruyuki@waseda.jp
[2] PRESTO, Japan Science and Technology Agency (JST)

studies have revealed that hemin is bound within a narrow D-shaped hydrophobic cavity in subdomain IB with axial coordination of Tyr-161 to the central ferric ion and electrostatic interactions between the porphyrin propionates and a triad of basic amino acid residues (Arg-114, His-146 and Lys-190) (Figure 1).[9,10] In terms of the general hydrophobicity of this $\alpha$-helical heme pocket, the subdomain IB of HSA potentially has similar features to the heme binding site of Hb or Mb. However, if one reduces the HSA–hemin to obtain the ferrous complex, it is rapidly oxidized by $O_2$, even at low temperature, because HSA lacks the proximal histidine that enables the prosthetic heme group to bind $O_2$ and serves to regulate the $O_2$ binding affinity (Figure 1). In order to confer the $O_2$ binding capability to this naturally occurring hemoprotein, we have introduced a proximal histidine into the heme binding site of HSA by site-directed mutagenesis; it would provide axial coordination to the central ferrous ion of the heme and thereby promote $O_2$ binding.[11] Moreover, to modulate its $O_2$ binding affinity, we have added further modification to the distal side of the heme. The $O_2$ binding properties of several rHSA(mutant)–heme complexes have been characterized kinetically and compared to those of the natural Hb, Mb, and red blood cells (RBC). We have shown that our mutagenesis approach can create a new class of albumin-based artificial hemoprotein which would serve as an $O_2$ carrier.

## Results and Discussion

### Double-Mutations to Confer the $O_2$ Binding Capability

The detailed structure of the heme binding site in HSA revealed by crystallographic studies allows the design of mutagenesis experiments to construct a tailor-made heme pocket for $O_2$ binding.[9,10] In fact, Tyr-161 was the first candidate to introduce a proximal histidine (Figure 1). However, the Y161H mutation was not done because our simulation indicated that the distance from His-161 to the central Fe would be too great (4.0 Å). Instead, modeling experiments suggested that the favorable positions for the axial imidazole insertion would be Ile-142 (Figure 2a). The N(histidine)–Fe distance was estimated as 2.31 Å for H142 (compared to 2.18 Å for Mb). We therefore designed a recombinant HSA (rHSA) double-mutant I142H/Y161L [=rHSA(HL)].

The specific mutations were introduced into the HSA coding region in the plasmid vector (pHIL-D2 HSA) using the QuikChange mutagenesis kit (Stratagene), and clones were expressed in the yeast *Pichia pastoris* (Invitrogen Corp.). The rHSA–hemin complexes were prepared funda-

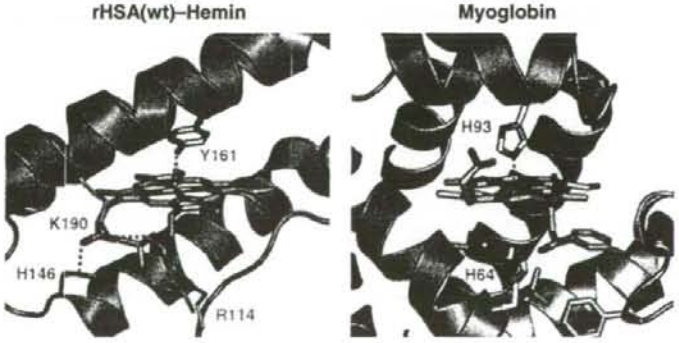


*Figure 1.*
Heme pocket structure in subdomain IB of HSA (left; 1O9X from ref. [9]) and heme pocket structure of Mb (1MBO).

 